Modeling hyperelasticity in non equilibrium multiphase flows

Sarah Hank, Nicolas Favrie, Jacques Massoni

Modeling hyperelasticity in non equilibrium multiphase flows

Sarah Hank, Nicolas Favrie and Jacques Massoni

May 17, 2016

Abstract

The aim of this article is the construction of a multiphase hyperelastic model. The Eulerian formulation of the hyperelasticity represents a system of 14 conservative partial differential equations submitted to stationary differential constraints. This model is constructed with an elegant approach where the stored energy is given in separable form. The system admits 14 eigenvalues with 7 characteristic eigenfields. The associated Riemann problem is not easy to solve because of the presence of 7 waves. The shear waves are very diffusive when dealing with the full system. In this paper, we use a splitting approach to solve the whole system using 3 sub-systems. This method reduces the diffusion of the shear waves while allowing to use a classical approximate Riemann solver. The multiphase model is obtained by adapting the discrete equations method. This approach involves an additional equation governing the evolution of a phase function relative to the presence of a phase in a cell. The system is integrated over a multiphase volume control. Finally, each phase admits its own equations system composed of three sub-systems. One and three dimensional test cases are presented.

Keywords: Hyperelasticity, Discrete Equation Method, Godunov type method

1 Introduction

Solid-fluid interaction in cases of extreme deformation occurs in many fundamental and industrial applications: hypervelocity impact on satellites, blast effects on structure... In such problems, high pressure and high density ratio are present at the level of interfaces. Works by [20], [1] and others, showed the attractivity of the diffuse interface approach to model interface between ideal compressible fluids having different thermodynamic features. This kind of model is reminiscent of the multiphase flow model developped initialy by [3] for the multi-velocity models or [18] and [19] for the one velocity models. Diffuse interfaces method presents several advantages compared to a direct coupling of models of homogeneous fluids through a sharp interface. Using this kind of multiphase flow models, the same equations are solved everywhere by using the same numerical scheme. This is achieved by considering a negligible quantity of other phases even in pure phase. With such an approach, there is no need of interface tracking or mesh distortion. This kind of model can describe the dynamic generation of new interfaces without having to re-mesh the domain, destroy or create cells. The main drawback of the Eulerian diffuse interface approach, compared to the Lagrangian formulation, is that the interface are not stiff. Indeed, the 'mixture cells' are always present at the vicinity of moving interfaces. The thickness of the 'mixture region' increases in time thus, depending on the treated problem, the method can only be used for short physical times.

This approach has been extended in [33] for the phase transition and in [9], [8], [27] for the interaction between elastoplastic solids and fluids dimension for a one-velocity model. Such one-velocity approach is limited to applications where no gas permeation is present, even if it can model various situations. This restricts the application domains. Moreover, the treatment of sliding interfaces is not straightforward. Another default of such approach is that the model is also one-pressure. Thus, it is unable to deal with different pressures in the mixture phase and then, limits the application for fracture treatment. The influence of the inertial effects and the different pressure between the gas in the inclusion and the solid

on the results of spaliation experiments is highlighted in [6]. In this paper, we propose an extension to multi-pressures and multi-velocities model in the case of hyperelastic solids.

Hyperelasticity model have been intensively studied in the past few years [16], [25] [21] and others. In this paper, we consider a modified conservative formulation in the case of isotropic solids ([15]). The specific stored energy is taken in separable form [13]. The internal energy is the addition of an hydrodynamic part, depending on the density and on the specific entropy, and an elastic part depending on the reduced Finger tensor.

$$e(\mathbf{G},\eta) = e^h(|\mathbf{G}|,\eta) + e^e(\mathbf{G}) \tag{1}$$

with $\mathbf{G} = \mathbf{B}^{-1}$ is the Finger tensor, and $\mathbf{B}$ is the Cauchy-Green deformation tensor, $\mathbf{g} = \mathbf{G}|\mathbf{G}|^{-1/3}$ is the reduced Finger tensor. Such a formulation of the internal energy implies that the shear part of the energy is unaffected by volume change, then adapted to pure fluids computations also. This model is hyperbolic for a suitable choice of the Equation of State (EOS) (See [28] and [14] for details). In such a case, the Riemann problem involves 7 characteristics waves which make its resolution complex. This resolution has been studied in details in [22], where a volume energy corresponding to a polynomial form of the deformation tensor is used. An exact solution of the hyperelastic Riemann problem has been provided for the simplified case of the piston problem in [28]. Although the Riemann problem can be solve numerically, this resolution is far too complex to be used in a practical numerical code. Approximate solvers have been built to capture the seven waves ([4, 15, 34]) but shear waves present a significant numerical diffusion. To circumvent this difficulty, a splitting procedure has been developed in [8]. Exact solvers are accessible, nevertheless a simple approximate Riemann solver may capture shear waves accurately.

In this paper, the hyperelastic model is splitted in 3 sub-systems. The first sub-system deals with the longitudinal waves while the two others deal with transverse (or shear) waves. Moreover, this splitting procedure is able to preserve the stationary constraint.

In order to get the multiphase formulation, we follow the *Discrete Equation Methods* developed and detailed in [2] or [32]. The multiphase model is obtained by adding a phase function equation and integrating each sub-systems equation weigthed by this fonction over a multiphase control volume. The integration leads to a discrete model: the evolution of each phase is taken into account by its own set of equations. The closure is realized by using a specific EOS per phase. In section 2, the hyperelastic equations are presented in the case of pure solid. The decomposition in sub-system is also presented. In section 3, the 'Discrete equation method' is applied to build the multiphase flow model. Then in section 4 the numerical treatment of the model is addressed. Numerical results in one-dimension of space are presented in section 5. Multi-dimensional examples are presented in section 6. Conclusion is addressed in section 7.

2 Governing equations: hyperelastic model

2.1 Equations for pure solids

Regarding the Eulerian formulation of hyperelasticity for isotropic solids ([16],[25] and others), we follow [15] for a modified presentation of these equations:

$$\begin{cases} \dfrac{\partial \rho}{\partial t} + \nabla.(\rho \mathbf{u}) = 0 \\ \dfrac{\partial \rho \mathbf{u}}{\partial t} + \nabla.(\rho \mathbf{u} \otimes \mathbf{u} - \boldsymbol{\sigma}) = 0 \\ \dfrac{\partial \rho E}{\partial t} + \nabla.(\rho E \mathbf{u} - \boldsymbol{\sigma}\mathbf{u}) = 0 \\ \dfrac{\partial \mathbf{e}^\beta}{\partial t} + \nabla.(\mathbf{e}^\beta \mathbf{u}) = 0, \quad \text{curl}(\mathbf{e}^\beta), \quad \text{with } \beta = 1,2,3 \end{cases} \tag{2}$$

Where ρ is the density of the material, $\mathbf{u} = (u, v, w)^T$ is the material velocity and E is the total energy of the system which corresponds to the sum of kinetic and internal energies. The closure of the system

is obtained with an internal energy expressed in separated form [9]:

$$E = \frac{\|\mathbf{u}\|^2}{2} + e^h(\rho,\eta) + e^e(\mathbf{g}), \qquad \mathbf{g} = \frac{\mathbf{G}}{|\mathbf{G}|^{1/3}},$$

e^h is the hydrodynamic part of the internal specific energy while e^e is the elastic part. $\mathbf{G}$ designates the Finger tensor, $\mathbf{g}$ represents the reduced Finger tensor. η is the specific entropy. The Finger tensor is a function of the deformation gradient $\mathbf{F}$ which is expressed as a function of the cobasis $\mathbf{e}^\beta = (\mathbf{e}^1, \mathbf{e}^2, \mathbf{e}^3)$,

$$\mathbf{F}^{-T} = (\mathbf{e}^1, \mathbf{e}^2, \mathbf{e}^3), \qquad \mathbf{G} = \mathbf{F}^{-T}\mathbf{F}^{-1} \implies \mathbf{G} = \sum_{\beta=1}^{3} \mathbf{e}^\beta \otimes \mathbf{e}^\beta.$$

At initial time, the cobasis corresponds to the Cartesian basis $(\mathbf{i}, \mathbf{j}, \mathbf{k})$. $\boldsymbol{\sigma}$ is the Cauchy stress tensor and can be expressed as the variation of the internal specific energy $e = e^h + e^e$:

$$\boldsymbol{\sigma} = -2\rho \frac{\partial e}{\partial \mathbf{G}} \mathbf{G}. \tag{3}$$

The separable form of the internal energy allows the following expression for the Cauchy stress tensor:

$$\boldsymbol{\sigma} = \mathbf{S} - p\mathbb{I}, \text{ with } \boldsymbol{S} = -2\rho \frac{\partial \mathrm{e^e}}{\partial \mathbf{G}} \mathbf{G}, \text{ and } \mathrm{p} = -\rho^2 \frac{\partial \mathrm{e^h}(\rho,\eta)}{\partial \rho}. \tag{4}$$

$\mathbf{S}$ is the deviatoric part of the Cauchy stress tensor. Let us remark that the pressure p is a function of the hydrodynamic part of the internal energy only. In this paper, we use the following expression for the elastic energy which depends on the two first invariants of the reduced Finger tensor:

$$e^e(\mathbf{g}) = \frac{\mu}{4\rho_0}\left(\frac{(1-2a)}{3} j_1^2 + a j_2 + 3(a-1)\right), \quad j_1 = tr(\mathbf{g}), \quad j_2 = tr(\mathbf{g^2}), \tag{5}$$

ρ_0 designates the reference density of the material, μ its shear modulus. Features of the elastic energy (5) has been studied in [14] where authors proved the rank-one convexity and have shown that this one-parameter family of equations of state contains the neo-Hookean solids (if a=-1). The deviatoric part of the Cauchy stress tensor can be expressed using expression (5):

$$\mathbf{S} = -\mu \frac{\rho}{\rho_0}\left(\frac{1-2a}{3} j_1 \left(\mathbf{g} - \frac{j_1}{3}\mathbb{I}\right) + a\left(\mathbf{g}^2 - \frac{j_2}{3}\mathbb{I}\right)\right). \tag{6}$$

For the hydrodynamic part of the internal energy, any convex equation of state (as function of $\tau = 1/\rho$ and η) can be considered. In this paper, the Stiffened gas equation of state [29] is used, that fulfill all conditions without loss of generality:

$$e^h(\rho, p) = \frac{P + \gamma P_\infty}{\rho(\gamma - 1)}, \tag{7}$$

where γ (dimensionless) and P_∞ (equivalent to a pressure) form a couple of parameters, characterizing the considered material. Let us introduce, $\mathbf{a}^\beta = (a^1, a^2, a^3)$, $\mathbf{b}^\beta = (b^1, b^2, b^3)$ and $\mathbf{c}^\beta = (c^1, c^2, b^3)$ such that $\mathbf{e}^\beta = (a^\beta, b^\beta, c^\beta)$. These definitions allow to express the Finger tensor $\mathbf{G}$:

$$\mathbf{G} = \begin{pmatrix} \|\mathbf{a}\|^2 & \mathbf{a}.\mathbf{b} & \mathbf{a}.\mathbf{c} \\ \mathbf{a}.\mathbf{b} & \|\mathbf{b}\|^2 & \mathbf{b}.\mathbf{c} \\ \mathbf{a}.\mathbf{c} & \mathbf{b}.\mathbf{c} & \|\mathbf{c}\|^2 \end{pmatrix}.$$

The last equation of system (2), describing the cobasis deformation, is written under conservative form. Nevertheless, to guaranty the hyperbolicity of the model the cobasis equation should be rewritten and used under the non-conservative form:

$$\frac{\partial \mathbf{e}^\beta}{\partial t} + \left(\frac{\partial \mathbf{e}^\beta}{\partial \mathbf{x}}\right)\mathbf{u} + \left(\frac{\partial \mathbf{u}}{\partial \mathbf{x}}\right)^T \mathbf{e}^\beta = 0, \quad \beta = 1, 2, 3. \tag{8}$$

System (2) is hyperbolic with 14 eigenvalues associated to seven characteristic directions: 2 longitudinal waves, 4 shear waves and a contact discontinuity. The hyperbolicity depends on the value of the parameter of the elastic energy (noted a). [26] and [14] proved that the system is hyperbolic for any value of a in the whole domain such that $-1 < a < 0.5$. In order to simplify the resolution of the Riemann problem -involving seven waves-, a splitting procedure has been proposed in [8]. This decomposition is described hereafter.

2.2 Model decomposition

System (2) can be splitted in 3 sub-systems. Each of them verifies the following properties (see [8] for details):

- The sub-systems are hyperbolic.
- The sub-systems are conservative.
- The sub-systems admit the energy equation compatible with the entropy equation.
- The sum of each sub-system solves the full system (2).

2.2.1 Sub-system 1

This first sub-system describes the longitudinal waves and the transport of the variables. These equations deal with the traction and the compression in the solid. They are similar to the Euler equations for compressible fluids with geometrical variables:

$$\left\{\begin{array}{l} \dfrac{\partial \rho}{\partial t} + \dfrac{\partial (\rho u)}{\partial x} = 0 \\ \dfrac{\partial \rho u}{\partial t} + \dfrac{\partial (\rho u^2 - \sigma_{11})}{\partial x} = 0 \\ \dfrac{\partial \rho v}{\partial t} + \dfrac{\partial (\rho uv - \sigma_{21})}{\partial x} = 0 \\ \dfrac{\partial \rho w}{\partial t} + \dfrac{\partial (\rho uw - \sigma_{31})}{\partial x} = 0 \\ \dfrac{\partial \rho E}{\partial t} + \dfrac{\partial (\rho Eu - \sigma_{11} u)}{\partial x} = 0 \\ \dfrac{\partial \mathbf{a}^\beta}{\partial t} + \dfrac{\partial (\mathbf{a}^\beta u)}{\partial x} = 0 \\ \dfrac{\partial \mathbf{b}^\beta}{\partial t} + u \dfrac{\partial \mathbf{b}^\beta}{\partial x} = 0 \\ \dfrac{\partial \mathbf{c}^\beta}{\partial t} + u \dfrac{\partial \mathbf{c}^\beta}{\partial x} = 0 \end{array}\right. \tag{9}$$

This last system admits 14 eigenvalues associated to 14 eigenvectors and is hyperbolic if the full system is hyperbolic. This sub-system admits the following eigenvalues :

$$\begin{array}{c} \lambda_1 = u, \\ \lambda_{2,3} = u \pm \sqrt{\dfrac{\partial p}{\partial \rho} - \dfrac{\partial S_{11}}{\partial \rho} - \dfrac{1}{\rho} \dfrac{\partial S_{11}}{\partial \mathbf{a}} . \mathbf{a}} \ , \end{array}$$

λ_1 is of multiplicity 12. The jump relations are similar to those of Euler equations whose the normal stress tensor replaces the pressure. Jump relations for the cobasis are trivial. The Riemann problem can be solved in a simple way, by using a classical HLLC solver for example [35].

2.2.2 Sub-systems 2 and 3

Sub-systems 2 and 3 are similar and uncoupled, they can be processed simultaneously:

$$\left\{\begin{array}{l} \dfrac{\partial \rho}{\partial t} = 0 \\ \dfrac{\partial \rho u}{\partial t} = 0 \\ \dfrac{\partial \rho v}{\partial t} - \dfrac{\partial(\sigma_{12})}{\partial x} = 0 \\ \dfrac{\partial \rho w}{\partial t} = 0 \\ \dfrac{\partial \rho E}{\partial t} - \dfrac{\partial(\sigma_{12} v)}{\partial x} = 0 \\ \dfrac{\partial \mathbf{a}^\beta}{\partial t} + \mathbf{b}^\beta \dfrac{\partial v}{\partial x} = 0 \\ \dfrac{\partial \mathbf{b}_k^\beta}{\partial t} = 0 \\ \dfrac{\partial \mathbf{c}_k^\beta}{\partial t} = 0 \end{array}\right. , \qquad \left\{\begin{array}{l} \dfrac{\partial \rho}{\partial t} = 0 \\ \dfrac{\partial \rho u}{\partial t} = 0 \\ \dfrac{\partial \rho v}{\partial t} = 0 \\ \dfrac{\partial \rho w}{\partial t} - \dfrac{\partial(\sigma_{13})}{\partial x} = 0 \\ \dfrac{\partial \rho E}{\partial t} - \dfrac{\partial(\sigma_{13} w)}{\partial x} = 0 \\ \dfrac{\partial \mathbf{a}^\beta}{\partial t} + \mathbf{c}^\beta \dfrac{\partial w}{\partial x} = 0 \\ \dfrac{\partial \mathbf{b}_k^\beta}{\partial t} = 0 \\ \dfrac{\partial \mathbf{c}_k^\beta}{\partial t} = 0 \end{array}\right. . \tag{10}$$

These two sub-models describe the propagation of shear waves. Each of them admits 14 eigenvalues and 3 characteristic velocities:

- Sub-system 2:

$$\lambda_{1,2} = \pm \sqrt{-\frac{1}{\rho} \frac{\partial S_{12}}{\partial \mathbf{a}} . \mathbf{b}} , \qquad \lambda_3 = 0.$$

- Sub-system 3:

$$\lambda_{1,2} = \pm \sqrt{-\frac{1}{\rho} \frac{\partial S_{13}}{\partial \mathbf{a}} . \mathbf{c}} , \qquad \lambda_3 = 0.$$

The Rankine-Hugoniot relations are very simple and it is possible, as previously, to consider an HLLC type solver with a motionless contact discontinuity.

3 Multiphase governing equations

The aim of this paper is to build a multiphase flow model including hyperelasticity. In [9] is proposed a one-velocity model. In this paper, we propose a fully out-of-equilibrium model whose each phase admits its own velocity and its own pressure. We follow here the *discrete equations method*, first developed in [2] and detailed in [23], [30], [32]. The *discrete equations method* (DEM) consists in the circulation of information between several equations systems, each of them governing the evolution of pure phases. In particular, the ability of the DEM allows to treat simultaneously out of equilibrium zones in multiphase flows and interfaces, that impose locally equilibrium of pressures and normal velocities of each phase (interface conditions).

In order to provide a better understanding of the following steps, a brief summary of the DEM construction process is presented in the next section in the case of pure fluids.

3.1 Summary of DEM construction in the case of fluid-fluid interactions

To build the flow model, the DEM considers a system of conservation laws (mass impulse and total energy) for each phase. Each system is written under the conservative form:

$$\frac{\partial \mathbf{U}}{\partial t} + \frac{\partial \mathbf{F}}{\partial x} = 0 \tag{11}$$

where

$$\mathbf{U} = \begin{pmatrix} \rho \\ \rho\mathbf{u} \\ \rho E \end{pmatrix}, \qquad \mathbf{F} = \begin{pmatrix} \rho\mathbf{u} \\ \rho\mathbf{u}\otimes\mathbf{u} - \boldsymbol{\sigma} \\ \rho\mathbf{u}E - \boldsymbol{\sigma}\mathbf{u} \end{pmatrix}.$$

the system is closed by a suitable equation of state for each phase. Using the DEM approach, each pure phase equation is weighted by the phase function and then integrated over a control volume containing all the phases (see [23], [2] for details). An example of multiphase control volume is presented in Figure 1 (involving morely two phases for the sake of simplicity).

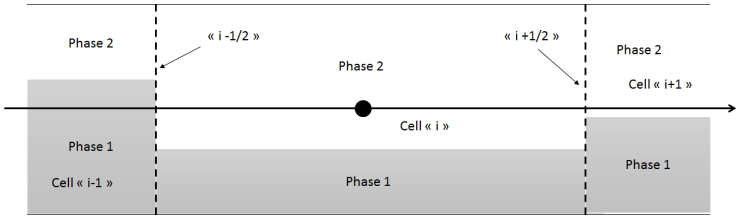

Figure 1: Control volume (V) in the case of multiphase flow (with 2 components).

As explained in [2], the use of an indicator variable χ_k becomes necessary to distinguish the phases and build the multiphase flow model. This indicator admits two possible values for each point inside the volume (V): 1 if the point is inside a given phase k and 0 elsewhere. This indicator follows the transport equation:

$$\frac{\partial \chi_k}{\partial t} + \nu_x \frac{\partial \chi_k}{\partial x} = 0.$$

where ν_x represents the local interface velocity. This equation reflects the correspondence between the Eulerian coordinates and the Lagrangian coordinates.
A multiplication of system (11) by χ_k for each phase k leads to:

$$\chi_k \frac{\partial \mathbf{U}}{\partial t} + \chi_k \frac{\partial \mathbf{F}}{\partial x} = 0,$$

and one can finally get:

$$\frac{\partial \chi_k \mathbf{U}}{\partial t} + \frac{\partial \chi_k \mathbf{F}}{\partial x} = (\mathbf{F} - \nu_x \mathbf{U}) \frac{\partial \chi_k}{\partial x}. \tag{12}$$

Denoting $\mathbf{F}^{Lag} = \mathbf{F} - \nu_x \mathbf{U}$ and taking into account the indicator equation, the final sytem is in the form:

$$\frac{\partial \chi_k \mathbf{U_k}}{\partial t} + \frac{\partial \chi_k \mathbf{F_k}}{\partial x} = \mathbf{F_k}^{Lag} \frac{\partial \chi_k}{\partial x} \tag{13}$$

where:

$$\mathbf{U_k} = \begin{pmatrix} 1 \\ \rho \\ \rho\mathbf{u} \\ \rho E \end{pmatrix}_k, \qquad \mathbf{F_k} = \begin{pmatrix} 0 \\ \rho\mathbf{u} \\ \rho\mathbf{u}\otimes\mathbf{u} + p\mathbf{I} \\ \rho\mathbf{u}E + p\mathbf{u} \end{pmatrix}_k, \qquad \mathbf{F_k}^{Lag} = \mathbf{F_k} - \nu_x \mathbf{U_k}.$$

To summarize, the DEM process involves three steps for the direct integration over the control volume of the solutions of interfaces problems :

- Phase selection by the indicator function
- Riemann problem solution at the interfaces between each pair of phases
- Direct average over space and time of Riemann problem solutions (Godunov's type scheme in each sub-volume)

$$\int_t \int_V \left(\frac{\partial \chi_k \mathbf{U_k}}{\partial t} + \frac{\partial \chi_k \mathbf{F_k}}{\partial x} \right) dV dt = \int_t \int_V \left(\mathbf{F_k}^{Lag} \frac{\partial \chi_k}{\partial x} \right) dV dt. \tag{14}$$

The integration on the control volume is detailed in [23], the resulting discrete equations are then obtained:

$$\alpha_k \mathbf{U}_{ki}^{n+1} = \alpha_k \mathbf{U}_{ki}^{n+1} + \frac{\Delta t}{\Delta x} \left\{ \begin{array}{c} -\left(\sum_{l,m} \{ S \chi_k^* \mathbf{F}^* \}_{lm,i+1/2} - \sum_{l,m} \{ S \chi_k^* \mathbf{F}^* \}_{lm,i-1/2} \right) \\ + \left(\sum_{l,m} \{ S [\chi_k]^* \mathbf{F}^{Lag,*} \}_{lm,i+1/2} + \sum_{l,m} \{ S [\chi_k]^* \mathbf{F}^{Lag,*} \}_{lm,i-1/2} \right) \end{array} \right\} \quad (15)$$

where α_k denotes the volume fraction of the phase k. Variables with superscript '$*$' correspond to solutions of the Riemann problem. S_{lm} represents the contact surface for each pair of fluids (or solids) in contact. Their expressions are obtained following simple arguments provided in [31]. Table 1 contains the values of these surfaces in the particular case of two-phase flow (for the cell boundary $i+1/2$). In such a case, $l \in \{1,2\}$ and $m \in \{1,2\}$. $\chi^*_{k,lm}$ represents the phase function of phase k for the same pair of fluid, their values are reported in Table 1.

Table 1: The different configurations for Eulerian fluxes at cell boundary $i+1/2$ for $k=1$.

Contact	Surface	Eulerian flux	Phase function χ_1^*
1-1	$S_{11} = Min(\alpha_{1,i}, \alpha_{1,i+1})$	F_{11}^*	$\chi^*_{1,11} = 1$
1-2	$S_{12} = Max(0, \alpha_{1,i} - \alpha_{1,i+1})$	F_{12}^*	$\chi^*_{1,12} = \left\{ \begin{array}{ll} 1 & \text{if } u^*_{12} > 0 \\ 0 & \text{otherwise} \end{array} \right.$
2-1	$S_{21} = Max(0, \alpha_{1,i+1} - \alpha_{1,i})$	F_{21}^*	$\chi^*_{1,21} = \left\{ \begin{array}{ll} 1 & \text{if } u^*_{12} < 0 \\ 0 & \text{otherwise} \end{array} \right.$
2-2	$S_{22} = Min(\alpha_{2,i}, \alpha_{2,i+1})$	F_{22}^*	$\chi^*_{1,22} = 0$

$[\chi_k]$ represents the jump of χ_k through an interface. The values of these jumps are resumed in Table 2 in the particular case of two-phase flows.

Table 2: The different configurations for Lagrangian fluxes at cell boundary $i+1/2$ for $k=1$.

Contact	Surface	Eulerian flux	Phase function χ_1^*
1-1	S_{11}	$F_{11}^{Lag,*}$	$[\chi_1]^*_{11} = -1$
1-2	S_{12}	$F_{12}^{Lag,*}$	$[\chi_1]^*_{12} = \left\{ \begin{array}{ll} -1 & \text{if } u^*_{12} > 0 \\ 0 & \text{otherwise} \end{array} \right.$
2-1	S_{21}	$F_{21}^{Lag,*}$	$[\chi_1]^*_{21} = \left\{ \begin{array}{ll} 1 & \text{if } u^*_{21} < 0 \\ 0 & \text{otherwise} \end{array} \right.$
2-2	S_{22}	$F_{22}^{Lag,*}$	$[\chi_1]^*_{22} = 0$

For an arbitrary number of fluids (or solids) the obtaining of surfaces $S_{k,lm}$ are detailed in [5], as well as the continuous model underlying which the general form is (k-th phase):

$$\left\{ \begin{array}{l} \dfrac{\partial \alpha_k}{\partial t} + \mathbf{u_I} \nabla \alpha_k = 0 \\ \dfrac{\partial (\alpha\rho)_k}{\partial t} + \nabla (\alpha \rho \mathbf{u})_k = 0 \\ \dfrac{\partial (\alpha\rho\mathbf{u})_\mathbf{k}}{\partial t} + \nabla (\alpha(\rho \mathbf{u} \otimes \mathbf{u} + p\mathbb{I}))_k = -p_I \nabla \alpha_k \\ \dfrac{\partial (\alpha\rho E)_k}{\partial t} + \nabla (\alpha(\rho E + p)\mathbf{u})_k = p_I \mathbf{u_I} \nabla \alpha_\mathbf{k} \end{array} \right. \quad (16)$$

Under the saturation condition: $\forall k \in \{1, N_{phases}\}, \alpha_k \in [0,1]$ *and* $\sum_k \alpha_k = 1$.

The interface variables p_I and $\mathbf{u}_I$ are fully determined by the Riemann problem solution. We take the

example of a pure hydrodynamic two-phase flow with gas (g) and liquid (l) (in 1D case):

$$\begin{cases} \dfrac{\partial \alpha_g}{\partial t} + u_I \dfrac{\partial \alpha_g}{\partial x} = 0 \\ \dfrac{\partial \alpha_g \rho_g}{\partial t} + \dfrac{\partial (\alpha_g \rho_g u_g)}{\partial x} = 0 \\ \dfrac{\partial \alpha_g \rho_g u_g}{\partial t} + \dfrac{\partial (\alpha_1 \rho_g u_g^2 + \alpha_g p_g)}{\partial x} = p_I \dfrac{\partial \alpha_g}{\partial x} \\ \dfrac{\partial \alpha_g \rho_g E_g}{\partial t} + \dfrac{\partial (\alpha_g \left(\rho_g E_g + p_g\right) u_g)}{\partial x} = p_I u_I \dfrac{\partial \alpha_g}{\partial x} \\ \dfrac{\partial \alpha_l \rho_l}{\partial t} + \dfrac{\partial (\alpha_l \rho_l u_l)}{\partial x} = 0 \\ \dfrac{\partial \alpha_l \rho_l u_l}{\partial t} + \dfrac{\partial (\alpha_l \rho_l u_l^2 + \alpha_l p_l)}{\partial x} = -p_I \dfrac{\partial \alpha_g}{\partial x} \\ \dfrac{\partial \alpha_l \rho_l E_l}{\partial t} + \dfrac{\partial (\alpha_l \left(\rho_l E_l + p_l\right) u_l)}{\partial x} = -p_I u_I \dfrac{\partial \alpha_g}{\partial x} \end{cases} \tag{17}$$

This system is hyperbolic (under minimal form) and totally out of equilibrium. It is obtained only by considering the fluxes travelling between adjacent cells of the mesh (*i.e.* at the level of mesh interfaces). Other phenomena such as relaxation may be regarded, involving terms that are internal for a cell.
We now interest in the addition of the elastic systems to the DEM formulation. The process is only detailed in the first space direction ($\mathbf{x}$), knowing that it is extensible exactly the same way in other dimensions.

3.2 Sub-systems in Multiphase Formulation

Each sub-system (9) and (10) consists in eight equations (scalar or vectorial). The first five equations of the sub-models express the conservation laws of mass, impulsion and total energy of the flow. The building process of the DEM, as described in the previous section, can be directly applied to those equations set. Then appears a supplementary relation concerning the volume fraction of the phase. In the following, we will call the associated variables of these equations the conservative variables (even if the governing equation of the volume fraction is not conservative). The last three equations constitute the cobasis governing equations and should be considered as geometric equations since they are derived from the Lagrangian coordinates and permit to compute the elasticity of the material.

3.2.1 Sub-system 1

The DEM can be applied directly to the conservative variables. The flow model is multiplied by the phase function χ_k then equations are integrated over the multiphase control volume:

$$\frac{\partial \chi_k \mathbf{U}}{\partial t} + \frac{\partial \chi_k \mathbf{F}}{\partial x} = (\mathbf{F} - \nu_x \mathbf{U}) \frac{\partial \chi_k}{\partial x}. \tag{18}$$

with

$$\mathbf{U} = \begin{pmatrix} 1 \\ \rho \\ \rho u \\ \rho v \\ \rho w \\ \rho E \end{pmatrix}, \qquad \mathbf{F} = \begin{pmatrix} 0 \\ \rho u \\ \rho u^2 - \sigma_{11} \\ \rho u v \\ \rho u w \\ \rho E u - \sigma_{11} u \end{pmatrix}.$$

Remember that the variation $\frac{\partial \chi_k}{\partial x}$ is non zero at the interface only. In the absence of reactive front, the interface velocity is equal to the fluid velocity ($\nu_x = u$):

$$\mathbf{F}^{Lag} = \mathbf{F} - \nu_x \mathbf{U} = \begin{pmatrix} -u \\ 0 \\ -\sigma_{11} \\ 0 \\ 0 \\ -\sigma_{11} u \end{pmatrix}.$$

Geometrical variables

The cobasis governing equations must be treated with a special care. Indeed, these geometrical equations and the evolution of this variables may depend on the topology of the flow. The link between the density and the geometrical variables $\rho = \rho_0 |\mathbf{G}|^{1/2}$ should be preserved. To ensure this, in [9], the cobasis equations are weighted by α^{n_β} with the following constraint:

$$n_\beta \geq 0, \quad \sum_{\beta=1}^{3} n_\beta = 1.$$

All the parameters were set to $n_\beta = 1/3$ in order to preserve the isotropy of the configuration. In the present work, the configuration is not anymore isotropic since we consider for example a stratified configuration in the **x**-direction. In such a configuration, there is no reason that the vector $\mathbf{b}^\beta$ and $\mathbf{c}^\beta$ change in the cell due to the transport of the material, because they are the derivative of the Lagrangian coordinates in the y and z direction. On the contrary, the component of $\mathbf{a}^\beta$ which corresponds to the gradient of the Lagrangian coordinates in the x-direction will depend on the material flow especially on the compression applied on the cells edges. In fact, it expresses another form of the mass conservation. It implies that this last vector should be weighted by the volume fraction. With such a process, the density is preserved and the full first sub-system can be written as follow for the "k-th" phase:

$$\begin{cases} \dfrac{\partial \alpha_k}{\partial t} + u_I \dfrac{\partial \alpha_k}{\partial x} = 0 \\ \dfrac{\partial (\alpha\rho)_k}{\partial t} + \dfrac{\partial (\alpha\rho u)_k}{\partial x} = 0 \\ \dfrac{\partial (\alpha\rho u)_k}{\partial t} + \dfrac{\partial (\alpha\rho u^2 - \alpha\sigma_{11})_k}{\partial x} = -\sigma_{11_I} \dfrac{\partial \alpha_k}{\partial x} \\ \dfrac{\partial (\alpha\rho v)_k}{\partial t} + \dfrac{\partial (\alpha\rho uv)_k}{\partial x} = 0 \\ \dfrac{\partial (\alpha\rho w)_k}{\partial t} + \dfrac{\partial (\alpha\rho uw)_k}{\partial x} = 0 \\ \dfrac{\partial (\alpha\rho E)_k}{\partial t} + \dfrac{\partial (\alpha\rho Eu - \alpha\sigma_{11} u)_k}{\partial x} = -\sigma_{11_I} u_I \dfrac{\partial \alpha_k}{\partial x} \\ \dfrac{\partial (\alpha \mathbf{a}^\beta)_k}{\partial t} + \dfrac{\partial (\alpha \mathbf{a}^\beta u)_k}{\partial x} = 0 \\ \dfrac{\partial \mathbf{b}_k^\beta}{\partial t} + u_k \dfrac{\partial \mathbf{b}_k^\beta}{\partial x} = 0 \\ \dfrac{\partial \mathbf{c}_k^\beta}{\partial t} + u_k \dfrac{\partial \mathbf{c}_k^\beta}{\partial x} = 0 \end{cases} \tag{19}$$

Thanks to the splitting procedure, there is no need to couple the two last equations of the previous system with the mass equation for the resolution. The resulting discrete model is similar to the model (15).

3.2.2 Sub-systems 2 and 3

When dealing with sub-system 2 and 3 (10), the interface velocity ν_x vanishes since there is no transport: $\nu_x = 0$, since transport has already been calculated in the previous system. Then, the phase function

follows:

$$\frac{\partial \chi_k}{\partial t} = 0.$$

This implies that the expressions of the lagrangian fluxes for sub-systems 2 and 3 are the same as the eulerian flux. As for the previous sub-model 1 (system (22)), each equation of system (2) is weighted by the indicator function except the last two. Sub-systems 2 and 3 can be solved simultaneously and the same procedure is applied. Then one can write:

$$\frac{\partial \chi_{\mathbf{k}} \mathbf{U}}{\partial t} + \frac{\partial \chi_k \mathbf{F}}{\partial x} = (\mathbf{F} - \nu_x \mathbf{U}) \frac{\partial \chi_k}{\partial x}$$

with $\mathbf{U}$, the conservative variables vector and $\mathbf{F}$ the flux vector:

$$\mathbf{F} = \begin{pmatrix} 0 \\ 0 \\ 0 \\ 0 \\ -\sigma_{12} \\ 0 \\ -\sigma_{12} v \end{pmatrix}, \text{for sub} - \text{system 2 and,} \qquad \mathbf{F} = \begin{pmatrix} 0 \\ 0 \\ 0 \\ 0 \\ 0 \\ -\sigma_{13} \\ -\sigma_{13} w \end{pmatrix}, \text{for sub} - \text{system 3.}$$

Thus this relation becomes:

$$\frac{\partial \chi_{\mathbf{k}} \mathbf{U}}{\partial t} + \frac{\partial \chi_k \mathbf{F}^{\mathbf{sub_2}}}{\partial x} + \frac{\partial \chi_k \mathbf{F}^{\mathbf{sub_3}}}{\partial x} = \mathbf{F}^{\mathbf{sub_2}} \frac{\partial \chi_k}{\partial x} + \mathbf{F}^{\mathbf{sub_3}} \frac{\partial \chi_k}{\partial x}$$

The sub-systems have to be integrated on the multiphase controle volume. The resulting discrete model for the conservative variables is:

$$\alpha_k \mathbf{U}_{ki}^{n+1} = \alpha_k \mathbf{U}_{ki}^{n+1} + \frac{\Delta t}{\Delta x} \left\{ \begin{array}{l} - \left(\sum_{l,m} \{ S \chi_k^* \mathbf{F}^{sub_2,*} \}_{lm,i+1/2} - \sum_{l,m} \{ S \chi_k^* \mathbf{F}^{sub_2,*} \}_{lm,i-1/2} \right) \\ + \left(\sum_{l,m} \{ S [\chi_k]^* \mathbf{F}^{sub_2,*} \}_{lm,i+1/2} + \sum_{l,m} \{ S [\chi_k]^* \mathbf{F}^{sub_2,*} \}_{lm,i-1/2} \right) \\ - \left(\sum_{l,m} \{ S \chi_k^* \mathbf{F}^{sub_3,*} \}_{lm,i+1/2} - \sum_{l,m} \{ S \chi_k^* \mathbf{F}^{sub_3,*} \}_{lm,i-1/2} \right) \\ + \left(\sum_{l,m} \{ S [\chi_k]^* \mathbf{F}^{sub_3,*} \}_{lm,i+1/2} + \sum_{l,m} \{ S [\chi_k]^* \mathbf{F}^{sub_3,*} \}_{lm,i-1/2} \right) \end{array} \right\} \quad (20)$$

The continuous model for the cobasis variables is obtained in a similar way as for the sub-system 1. The continuous model described by this last system is:

$$\left\{\begin{array}{l}
\dfrac{\partial \alpha_k}{\partial t} = 0 \\
\dfrac{\partial (\alpha\rho)_k}{\partial t} = 0 \\
\dfrac{\partial (\alpha\rho u)_k}{\partial t} = 0 \\
\dfrac{\partial (\alpha\rho v)_k}{\partial t} - \dfrac{\partial (\alpha\sigma_{12})_k}{\partial x} = -\sigma_{12_I}\dfrac{\partial \alpha_k}{\partial x} \\
\dfrac{\partial (\alpha\rho w)_k}{\partial t} - \dfrac{\partial (\alpha\sigma_{13})_k}{\partial x} = -\sigma_{13_I}\dfrac{\partial \alpha_k}{\partial x} \\
\dfrac{\partial (\alpha\rho E)_k}{\partial t} + \dfrac{\partial (-\alpha\sigma_{12}v)_k - \alpha\sigma_{13}w)_k}{\partial x} = -\sigma_{12_I}v_I\dfrac{\partial \alpha_k}{\partial x} - \sigma_{13_I}w_I\dfrac{\partial \alpha_k}{\partial x} \\
\dfrac{\partial (\alpha \mathbf{a}^\beta)_k}{\partial t} + (\alpha \mathbf{b}^\beta)_k\dfrac{\partial v_k}{\partial x} + (\alpha \mathbf{c}^\beta)_k\dfrac{\partial w_k}{\partial x} = 0 \\
\dfrac{\partial \mathbf{b}_k^\beta}{\partial t} = 0 \\
\dfrac{\partial \mathbf{c}_k^\beta}{\partial t} = 0
\end{array}\right. \tag{21}$$

One can note that the volume fraction in the cobasis equation can be removed.

3.2.3 Hyperbolicity

Each system is hyperbolic (since each phase model is hyperbolic). As there is an additional equation (for the volume fraction), the Jacobian matrix of each sub-model admits 15 eigenvalues and 15 eigenvectors (presented in Appendix). The characteristic speeds remain unchanged.

3.3 General model

The overall system solve the following multiphase flow model :

$$\left\{\begin{array}{l}
\dfrac{\partial \alpha_k}{\partial t} + u_I\dfrac{\partial \alpha_k}{\partial x} = 0 \\
\dfrac{\partial (\alpha\rho)_k}{\partial t} + \dfrac{\partial (\alpha\rho u)_k}{\partial x} = 0 \\
\dfrac{\partial (\alpha\rho u)_k}{\partial t} + \dfrac{\partial (\alpha\rho u^2 - \alpha\sigma_{11})_k}{\partial x} = -\sigma_{11_I}\dfrac{\partial \alpha_k}{\partial x} \\
\dfrac{\partial (\alpha\rho v)_k}{\partial t} + \dfrac{\partial (\alpha\rho uv)_k}{\partial x} + \dfrac{\partial (-\alpha\sigma_{12})_k}{\partial x} = -\sigma_{12_I}\dfrac{\partial \alpha_k}{\partial x} \\
\dfrac{\partial (\alpha\rho w)_k}{\partial t} + \dfrac{\partial (\alpha\rho uw)_k}{\partial x} + \dfrac{\partial (-\alpha\sigma_{13})_k}{\partial x} = -\sigma_{13_I}\dfrac{\partial \alpha_k}{\partial x} \\
\dfrac{\partial (\alpha\rho E)_k}{\partial t} + \dfrac{\partial (\alpha\rho Eu - \alpha\sigma_{11}u - \alpha\sigma_{12}v - \alpha\sigma_{13}w)_k}{\partial x} = -(\sigma_{11_I}u_I + \sigma_{12_I}v_I + \sigma_{13_I}w_I)\dfrac{\partial \alpha_k}{\partial x} \\
\dfrac{\partial (\alpha \mathbf{a}^\beta)_k}{\partial t} + \dfrac{\partial (\alpha \mathbf{a}^\beta u)_k}{\partial x} + (\alpha \mathbf{b}^\beta)_k\dfrac{\partial v_k}{\partial x} + (\alpha \mathbf{c}^\beta)_k\dfrac{\partial w_k}{\partial x} = 0 \\
\dfrac{\partial \mathbf{b}_k^\beta}{\partial t} + u_k\dfrac{\partial \mathbf{b}_k^\beta}{\partial x} = 0 \\
\dfrac{\partial \mathbf{c}_k^\beta}{\partial t} + u_k\dfrac{\partial \mathbf{c}_k^\beta}{\partial x} = 0
\end{array}\right. \tag{22}$$

This system can be solved directly by using the procedure presented in the next section. Since the exact Riemann solver is too complex to be used in numerical code, an approximate Riemann solver must be used. An adaptation of the HLLC solver [35] based on the Hugoniot relations was proposed in [15]. This solver is able to capture the 7 waves present in the Riemann problem even if it considers only three waves. Unfortunately, huge diffusion is present with such a solver. Another difficulty appears

when fluids are in contact with solids. The Riemann solver degenerates and the shear waves disapears on the fluid side of the interface. The treatment of such cases is not straightforward with the global system and will be discussed in detail for the sub-system 2. In the following, we will only discuss the numerical treatment of the splitting approach.

4 Numerical treatment

The principle of the *Discrete Equation Method* is to solve several Riemann problems between pure phases as presented in Figure 2. The resulting fluxes are then weighted by the contact surface between these fluids. The variables evolution is realized using a Godunov type scheme.

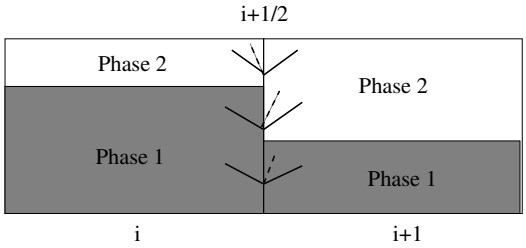

Figure 2: Riemann problem to solve between each phase.

4.1 Riemann problem for sub-system 1

The jump relations are those of pure fluids. The first sub-system is similar to the Euler equations in the case of multiphase flows with multiple transport equations along the particles trajectories. Exact Riemann solver could be used but we prefer to use a HLLC type solver [35]. Indeed, especially in the context of solids, complex equations of state may be necessary in order to describe accurately some problems, as Mie-Gruneisen type EOS for example. Then, it is not possible to find the exact solution of the Riemann problem.
The approximate HLLC Riemann solver considers two shock waves and a contact discontinuity as presented in Figure 3. This kind of Riemann solver has already shown its efficiency in [8] in the case of pure solids. We just recall here the jump relations. In the following we use the Davis approximation [7] concerning the extreme waves speeds D_L and D_R.

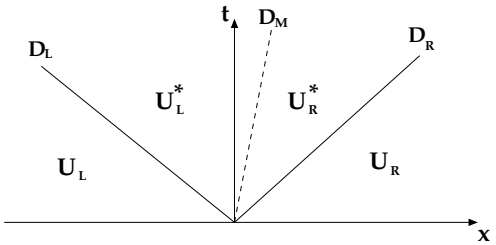

Figure 3: HLLC representation of the Riemann Problem.

Jump relations for the conservative variables.
The Rankine-Hugoniot relations across each wave (D_R,D_L,D_M) are :

$$\begin{aligned} \mathbf{F}_L^* - D_L \mathbf{U}_L^* &= \mathbf{F}_L - D_L \mathbf{U}_L \\ \mathbf{F}_R^* - D_R \mathbf{U}_R^* &= \mathbf{F}_R - D_R \mathbf{U}_R \\ \mathbf{F}_L^* - D_M \mathbf{U}_L^* &= \mathbf{F}_R^* - D_M \mathbf{U}_R^* \end{aligned}$$

with

$$\mathbf{F} = \left((\rho u)_k, (\rho u^2 - \sigma_{11})_k, (\rho uv)_k, (\rho uw)_k, (\rho uE - \sigma_{11} u)_k\right)^T$$
$$\mathbf{U} = (\rho_k, (\rho u)_k, (\rho v)_k, (\rho w)_k, (\rho E)_k)^T .$$

F and U represent respectively the flux vector and the vector of conservative variables. We can notice that jump relations for the physical variables are not affected by the hyperelasticity.

Jump relations for geometrical variables
The Rankine Hugoniot relations across the shock waves (D_R and D_L) lead to :

$$\begin{aligned} \left[a^\beta (u - D)\right] &= 0, \\ \left[b^\beta\right] &= 0, \\ \left[c^\beta\right] &= 0. \end{aligned}$$

Jump relation across the contact discontinuity:
The contact discontinuity can be localized in a pure phase or at the interface between two phases. Across this discontinuity, the jump of geometrical variables is arbitrary, the same way as for the density. For the flow variables, the interface relations will be:

$$\begin{aligned} \sigma^*_{11L} = \sigma^*_{11R} = \sigma^*_{11}, \\ u^*_l = u^*_r = u^*. \end{aligned}$$

All these fluxes must be weighted with the contact surface between the left and the right material. The HLLC solver gives the flux across cells edges. In order to solve system (22), additional fluxes have to be considered when solving a Riemann problem between two different materials. The concerned variables are the volume fraction, the momentum (in the **x** direction) and the total energy.

4.2 Riemann problem for Sub-system 2

In sub-system 2, there is no transport equation. If two solids are considered, the Riemann problem involves 3 waves with a zero velocity central wave. When interface between solids and fluids or pure fluids are present, some waves disappear. Indeed, the complete model is not anymore strictly hyperbolic and the cobasis equations are useless. Such configurations are represented in Figure (4).

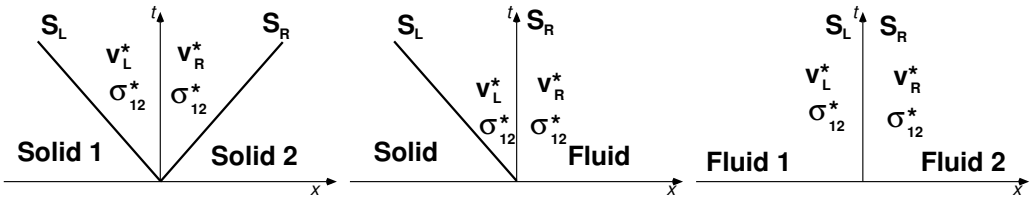

Figure 4: Three different possible configurations. At the contact discontinuity between two solids a transverse velocity jump may be present. When fluids are present, the velocity jump is arbitrary and the tangential stress σ^*_{12} is set to zero.

We will first detail the Riemann solver between two solids. In that case, two shock waves and a zero velocity central wave are considered. An HLLC type solver can again be used to solve the Riemann problem. One can express the Rankine Hugoniot relations associated to the sub-system 2.

Jump across the shock waves
The wave speeds D_R and D_L are evaluated using the Davis approximation [7]. The Rankine Hugoniot relations across the shock waves lead to:

$$\begin{aligned} [\rho_k] = 0, \quad [\rho_k u_k] = 0, \quad [\rho_k w_k] = 0, \\ [-\sigma_{12_k} - D\rho_k v_k] = 0, \\ [-\sigma_{12_k} v_k - D\rho_k E_k] = 0, \end{aligned} \tag{23}$$

for the flow variables, and to

$$\left[\mathbf{b}^{\beta} v_k - D\mathbf{a}^{\beta}\right] = 0,$$
$$\left[\mathbf{b}^{\beta}\right] = 0, \quad \left[\mathbf{c}^{\beta}\right] = 0,$$

for the geometrical variables.

Jump across the contact discontinuity:
Physically, two patterns can occur at the contact discontinuity. Indeed, the velocity field can be continuous, the two sides stick together, or the two sides of the interface can slide together with an arbitrary velocity. All the patterns between these two cases can also occur. In the following, we will consider that when the same phase is present at the interface the materials is continuous. The jump relations for the physical variables are:

$$[v] = 0, \quad [\sigma_{12}] = 0.$$

When two different phases are present, two possibilities can be chosen:

- There is no friction between the materials $\sigma_{12}^* = 0$ and the velocity jump is determined by the shock relations (23). In that case, two different velocities have to be defined v_R^* and v_L^* on the right and the left of the interface.
- There is adherence between the two phases and the jump relations are $[v] = 0$ and $[\sigma_{12}] = 0$.

For the other variables, the jump is always arbitrary in agreement with the shock jump relations. When a fluid is present (on one side or both sides of the interface), the shock jump are not anymore valid since the wave is absent. Indeed, when the shear modulus tends to zero, the wave speed also tends to zero and collapse to the interface. In the case, for example, where the fluid is on the right, we have at the contact dicontinuity $v_R^* = v_R$ and $\sigma_{11}^* = 0$. The velocity jump is arbitrary and if a solid is present on the left, the right star state is determined by the solid jump relations.

4.3 Numerical scheme

Once the solutions of the Riemann problems have been computed, fluxes can be expressed. A Godunov type scheme is used.

4.3.1 Sub-system 1

As the *discret equation method* corresponds to both a discret model and a numerical scheme, this last is the result of the integration on the controle volume, given by the expression (15). The numerical scheme for the geometrical variables is the following :

$$\begin{bmatrix} \alpha_k \mathbf{a}_k^{\beta} \\ \mathbf{b}_k^{\beta} \\ \mathbf{c}_k^{\beta} \end{bmatrix}^{n+1} = \begin{bmatrix} \alpha \mathbf{a}_k^{\beta} \\ \mathbf{b}_k^{\beta} \\ \mathbf{c}_k^{\beta} \end{bmatrix}^{n} - \frac{\Delta t}{\Delta x} \begin{bmatrix} \sum_{l,m} \{S\chi_k^*(\mathbf{a}_k^{\beta} u_k)^*\}_{lm,i+1/2} - \sum_{l,m} \{S\chi_k^*(\mathbf{a}_k^{\beta} u_k)^*\}_{lm,i-1/2} \\ (\mathbf{b}_k^{\beta} u_k)_{i+1/2}^* - (\mathbf{b}_k^{\beta} u_k)_{i-1/2}^* - \mathbf{b}_k^{\beta}(u_{k,i+1/2}^* - u_{k,i-1/2}^*) \\ (\mathbf{c}_k^{\beta} u_k)_{i+1/2}^* - (\mathbf{c}_k^{\beta} u_k)_{i-1/2}^* - \mathbf{c}_k^{\beta}(u_{k,i+1/2}^* - u_{k,i-1/2}^*) \end{bmatrix} \quad (24)$$

Fluxes at the cells edges are computed with an approximate Riemann solver. The same procedure is used to solve sub-systems 2 and 3 describing shear effects.

4.3.2 Sub-systems 2 and 3

The numerical scheme associated to sub-systems 2 and 3 is the result of the integration performed in a previous section. The scheme associated to the hydrodynamic variables is given by the expression (20).

The numerical scheme for the geometrical variables is given for both sub-models 2 and 3. $\mathbf{b}^\beta$ and $\mathbf{c}^\beta$ do not change during this step ($(\mathbf{b}_k^\beta)^{n+1}$=$(\mathbf{b}_k^\beta)^n$, $(\mathbf{c}_k^\beta)^{n+1}$=$(\mathbf{c}_k^\beta)^n$).

$$(\alpha_k \mathbf{a}_k^\beta)^{n+1} = (\alpha \mathbf{a}_k^\beta)^n - \frac{\Delta t}{\Delta x} \begin{pmatrix} \mathbf{b}_k^\beta \sum_{l,m} \left(\{S\chi_k^*(v_k)_L^*\}_{l,m,i+1/2} - \{S\chi_k^*(v_k)_R^*\}_{l,m,i-1/2} \right) \\ +\mathbf{c}_k^\beta \sum_{l,m} \left(\{S\chi_k^*(w_k)_L^*\}_{i+1/2} - \{S\chi_k^*(w_k)_L^*\}_{i-1/2} \right) \end{pmatrix} \tag{25}$$

If an interface is present, shear stresses at the interface must be expressed ($\sigma_{12I}, \sigma_{13I}$). Indeed, it is possible to consider sliding or adherence condition at the interface. In this work, only sliding condition is considered at the interface. So there is no shear interaction between two solids at an interface and we assume that the interface shear stresses vanishe. One can notice that the equation for the geometrical variable is not conservative due to the discontinuity of the velocity at the interface between two phases. When the sliding is possible, the Lagrangian coordinates of each phase are not linked anymore. Thus another phase should not create deformation in the phase at that time.

4.4 Summary

The numerical resolution can be summarized as follow :

1. Compute each contact surface between each phase.
2. Compute each Riemann problem between each phase for the sub-system 1
3. Evolve the conservative variables using the Godunov type scheme for sub-system 1
4. Compute each contact surface between each phase.
5. Compute each Riemann problem between each phase for the sub-system 2
6. Evolve the conservative variables using the Godunov type scheme for sub-system 2
7. Compute each Riemann problem between each phase for the sub-system 3
8. Evolve the conservative variables using the Godunov type scheme for sub-system 3
9. Return to step 1

5 One dimensional tests and validations

In the following test cases, we consider aluminium, copper, carbopol as perfectly elastic solid and air as a perfect gas. The parameters of the considered materials are resumed in Table 3.

Material	γ	P_∞ (Pa)	μ (Pa)	ρ_0 (kg/m^3)	a (eos parameter)
Aluminium	3.4	21.5 10^9	26 10^9	2700	0.5
Copper	4.2	34.2 10^9	92 10^9	8900	0.5
Carbopol	2.2	10^6	85	1020	0 and -1
Air	1.4	-	-	1.19	-

Table 3: Features of materials

5.1 Advection of a solid-gas interface

We consider a tube filled with solid aluminium at a density $\rho = 2700kg/m^3$ on the left and air with the density $\rho = 1kg/m^3$ on the right. The pressure $p = 0.1MPa$ is uniform in the whole domain as well as the velocity $u = 400m/s$. The domain length is $1m$ long. The interface is initially located at $x = 0.5m$. The initial configuration is presented in Figure 5. A 2000 cells mesh is used for the computation. The numerical results are represented in Figure 6 at time $t = 0.5ms$. This test shows that the numerical method is able to preserve mechanical equilibrium states in the presence of interface with a very large density ratio.

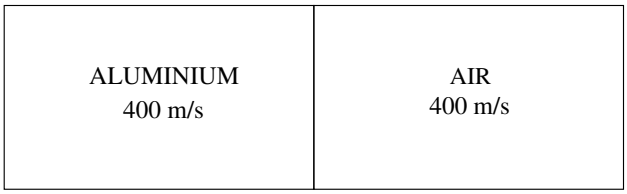

Figure 5: Initial configuration: a solid/gas interface is moving with a constant velocity.

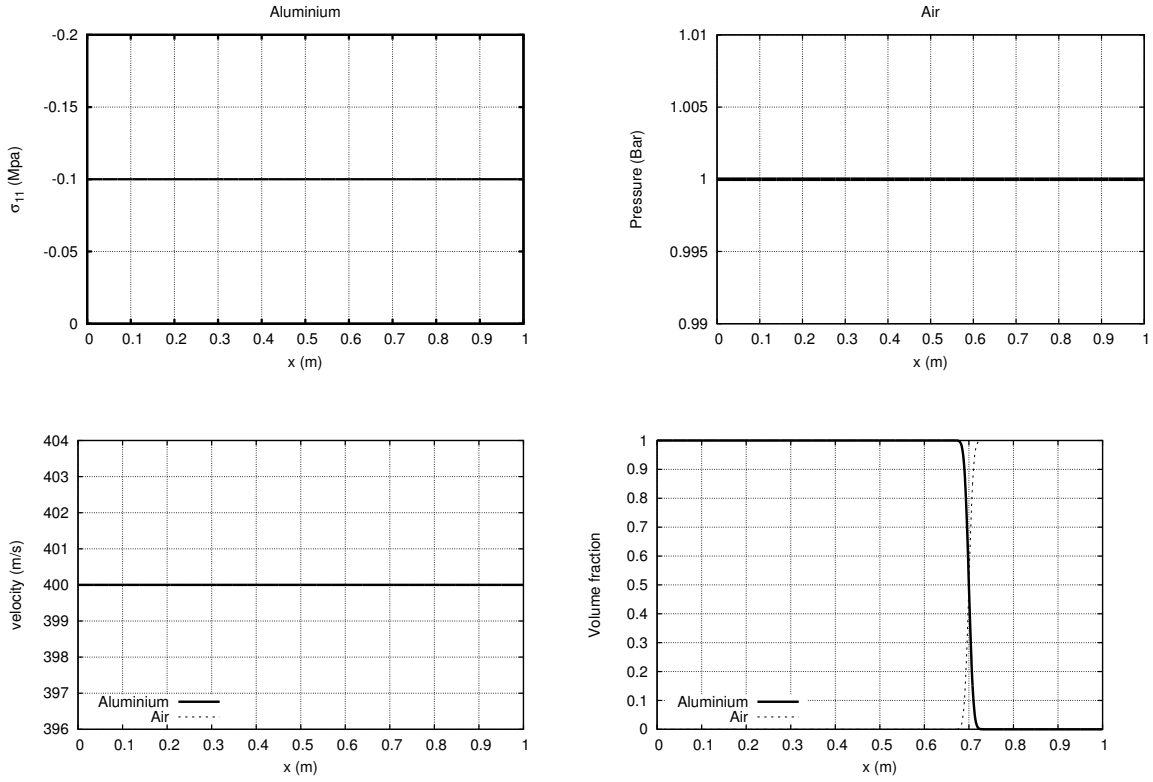

Figure 6: Advection test case: Visualisation of the normal stress of the Aluminum (Top left), the air pressure (Top right), velocities of both materials (bottom left) and the volume fraction of the components. All the variables are represented at time $t = 0.5ms$.

5.2 Impact between two elastic solids

In the following test case we consider the collision between two elastic solids. We consider copper moving at $400m/s$ with density $\rho = 8900kg/m^3$ on the left. On the right, we consider aluminium moving at $-200m/s$ with density $\rho = 2700kg/m^3$. At initial time, the two materials are at atmospheric pressure. The interface is located at abscissa $x = 0.5m$. The initial configuration is summarized in Figure 7. In each phase, a negligible amount of the other phase ($\alpha_{min} = 10^{-5}$) is present. Results are presented in Figures 8 and 9 at time $t = 50\mu s$ on a 2000 cells mesh.

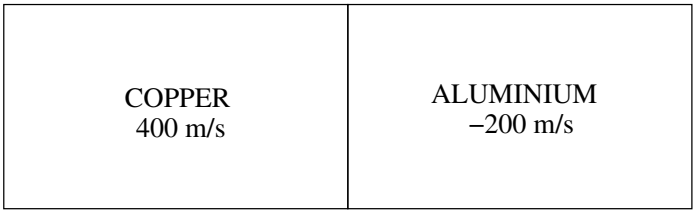

Figure 7: Initial configuration for the impact of two solids.

The mixture variables are defined as follow:

$$\sigma_{mix} = \sum_k \alpha_k \sigma_k, \quad u_{mix} = \sum_k Y_k u_k,$$

where Y_k is the mass fraction of phase k.

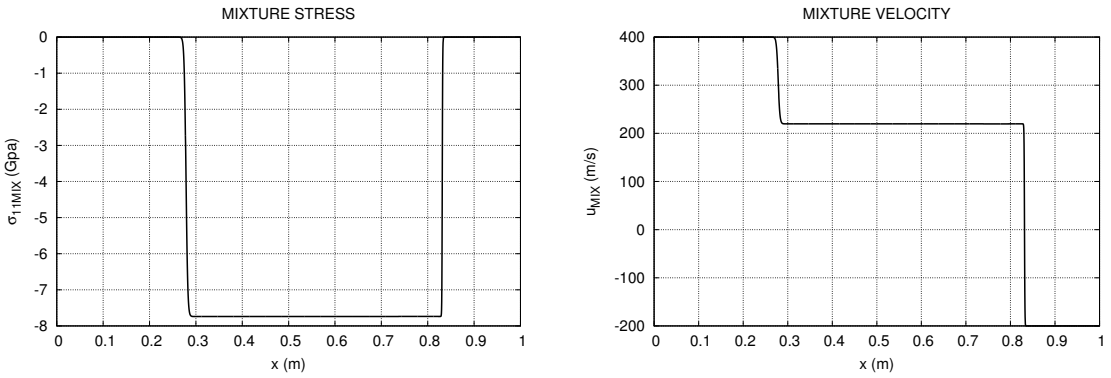

Figure 8: The mixture variables $\sigma_{mix} = \sum_k \alpha_k \sigma_k$ and $u_{mix} = \sum_k Y_k u_k$ are represented. The interface relations are satisfied: the normal stress and the normal velocity are continuous at the interface.

In this test, two shock waves propagate in each phase with different velocities. One can notice that no oscillation is present on the mixture variables at the interface. The continuity of the normal stress and the mixture velocity is preserved at the interface. One can notice that a pressure jump is present at the interface unlike when only pure fluids are present.

5.3 Shear Test

Initially, the normal velocity is set to zero as well as the shear stress. The whole domain is at atmospheric pressure. Only aluminium is considered in this test. At initial time, a tangential velocity discontinuity

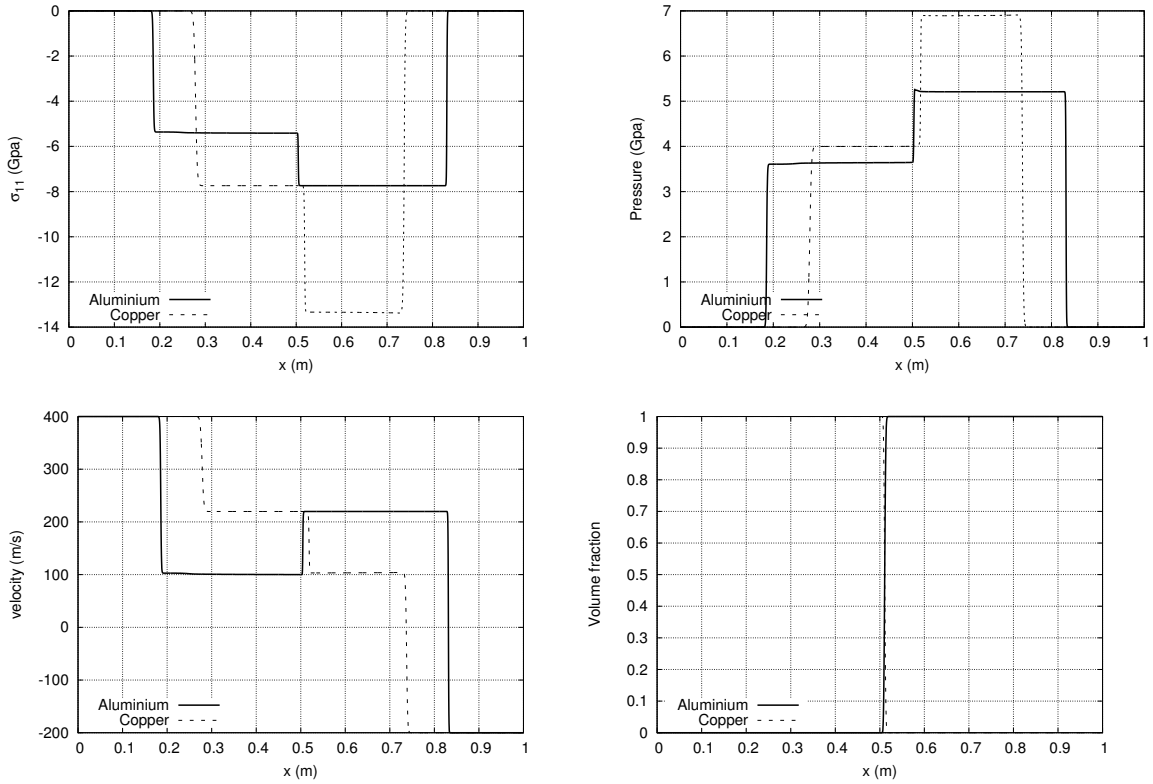

Figure 9: Impact between two solids. Results are presented at time $t = 50\mu s$ on a 2000 cells mesh. The phase characteristics are represented. On these figures, aluminium is represented with lines, copper is represented with dashed line.

($\delta v = 1000m/s$) is present at abscissa $x = 0.5m$. The initial configuration is presented in Figure 10. Aluminium has been used for this example. The domain is one meter long. Results are presented in Figure 11 at time $t = 50\mu s$ on a 2000 cells mesh. The exact solution ([8]) is represented with lines, the numerical results are represented with symbols. The solution corresponds to the propagation of two compression waves and two shear waves. Rarefaction is present in the shear waves. This test shows the ability of the numerical scheme to capture waves propagation in pure phase.

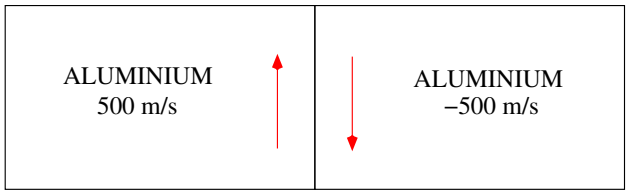

Figure 10: Initial configuration for the shear test. A tangential velocity jump $\delta v = 1000m/s$ is present at the interface.

5.4 Sliding between 2 solids

We consider here the sliding between 2 solids (copper and aluminium) at an interface. At initial time, all the materials are at atmospheric pressure. The normal velocity is set to $200m/s$ and a transverse

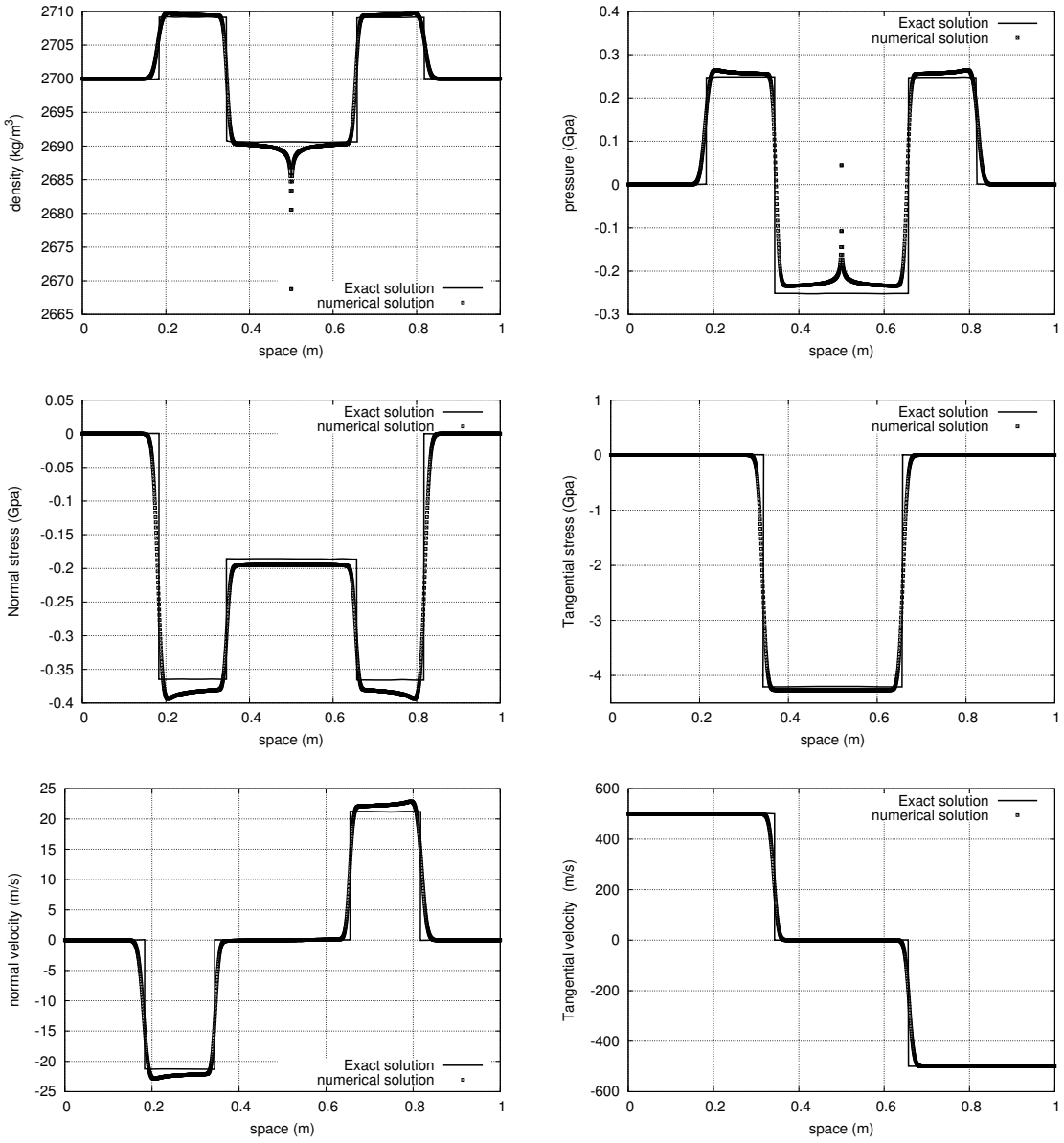

Figure 11: Shear test problem. Initially, a discontinuity of tangential velocity exists. Here are presented the profiles of density, pressure, normal stress, shear stress, normal velocity and tangential velocity at the instant t=50 μs.The exact solution proposed in [8] is represented in lines, the numerical solution obtained with a 2000 cells mesh is represented with symbols.

velocity discontinuity is present at the interface $\delta v = 100m/s$. The sliding is supposed to be perfect *i.e.* the tangential stress between the two phases is set to 0 in the Riemann problem. The domain is $1m$ long and the interface is located at abscissa $x = 0.5m$. Results are presented at time $t = 0.1ms$ in Figure 12. No oscillations are present at the interface. The transverse velocity jump between the two phases is preserved.

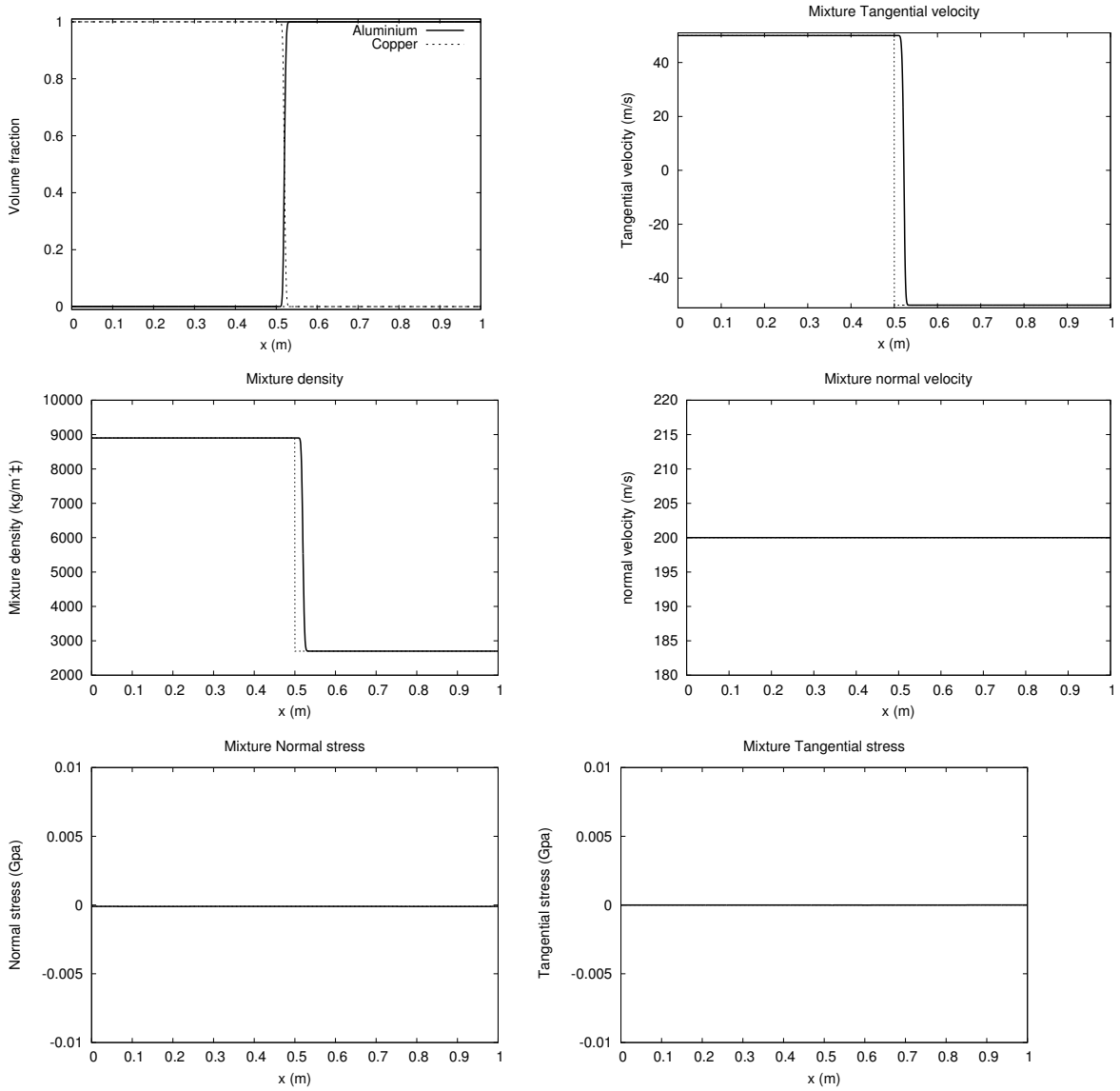

Figure 12: Sliding between two solids: the volume fraction of each solid is presented as well as the mixture variables at time $t = 0.1ms$. The tangential velocity jump is transported and preserved. There is no oscillation at the interface.

The numerical treatment of such a test is always a difficult issue. In Lagrangian codes, such problem needs complex algorithms (see for example [17]). For Eulerian codes, the issue was described in [9] and a special treatment was proposed. This treatment is not straightforward and the preservation of the momentum and the energy is difficult to guaranty. This test case show the ability of this new approach to deal with such problems without complex algorithm. The conservation properties are guaranteed by the scheme.

6 Multi-dimensional examples

Multi-dimensional extension of the method is direct. An analogous finite volume splitting procedure is used in each directions. The first step is the resolution of the system describing the traction-compression of the elastic body in the three directions (sub system 1). Then sub-systems 2 and 3 are solved simultaneously in each direction.

6.1 Impact of a projectile on a plate with high velocity

In this test, we consider the impact of a copper projectile ($0.1m \times 0.1m$) on a copper plate ($0.1m \times 0.1m$). The system is surrounded by air at atmospheric conditions. The initial velocity of the projectile is $u = 600\ m.s^{-1}$. The computation domain, described in Figure 13 is $0.5m \times 0.6m$ on a 1000×1200 cells mesh. The contact between the projectile and the plate is done initially, so there is no interface between both solids. Results are presented in Figure 14 at respective instants $t = 40\mu s$, $t = 70\mu s$, $t = 110\mu s$, $t = 200\mu s$, $t = 300\mu s$, $t = 490\mu s$ and $t = 700\mu s$. The copper volume fraction is represented on the bottom of each picture of the figure while the schlieren of the density is represented on the top of them. The plate oscillates during the time evolution and shock are transmitted from the solid to the air. This test shows the ability of the model to compute strong shock in 2D configuration.

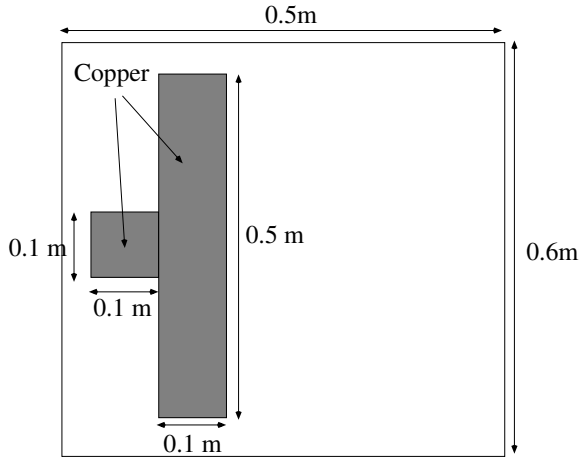

Figure 13: A copper projectile strikes a copper plate with a velocity $u = 600m/s$.

6.2 Comparison with experiment : impact of a jelly droplet

In the previous example, we consider a non-physical test case. Indeed, when such impact happens, lots of physics is present. Plasticity, fracture and many other phenomena can occur. Unlike metals, jelly like materials can remain elastic even for extreme deformation (100%-200%). This aspect has been studied by [24]. In this example, a cylindrical gel sample (Carbobol) of diameter L_0 impacting a rigid hydrophobic surface spreads over the surface until some limit size L_M and then a full elastic recoil is observed which may be followed by a complete rebound. We reproduce this quasi-reversible behaviour numerically. The initial configuration is depicted in Figure 15. The initial diameter is $L_0 = 0.012m$, the jelly cylinder high is $H = 0.008m$, and the initial velocity of the droplet is $v = -3m/s$. We use a 3D version of the numerical code with a $100 \times 100 \times 100$ cells mesh to compute the entire domain.

Materials features are given in Table 3. Two different values of the parameter a associated to the elastic equation of state are considered ($a = -1$ and $a = 0$). The results for the two parameters are compared in Figure 16. The droplet contours are plotted at different times. during the first instants ($t < 1.5ms$), the behaviour of the droplet is similar for the two values of the parameter a. Then, one

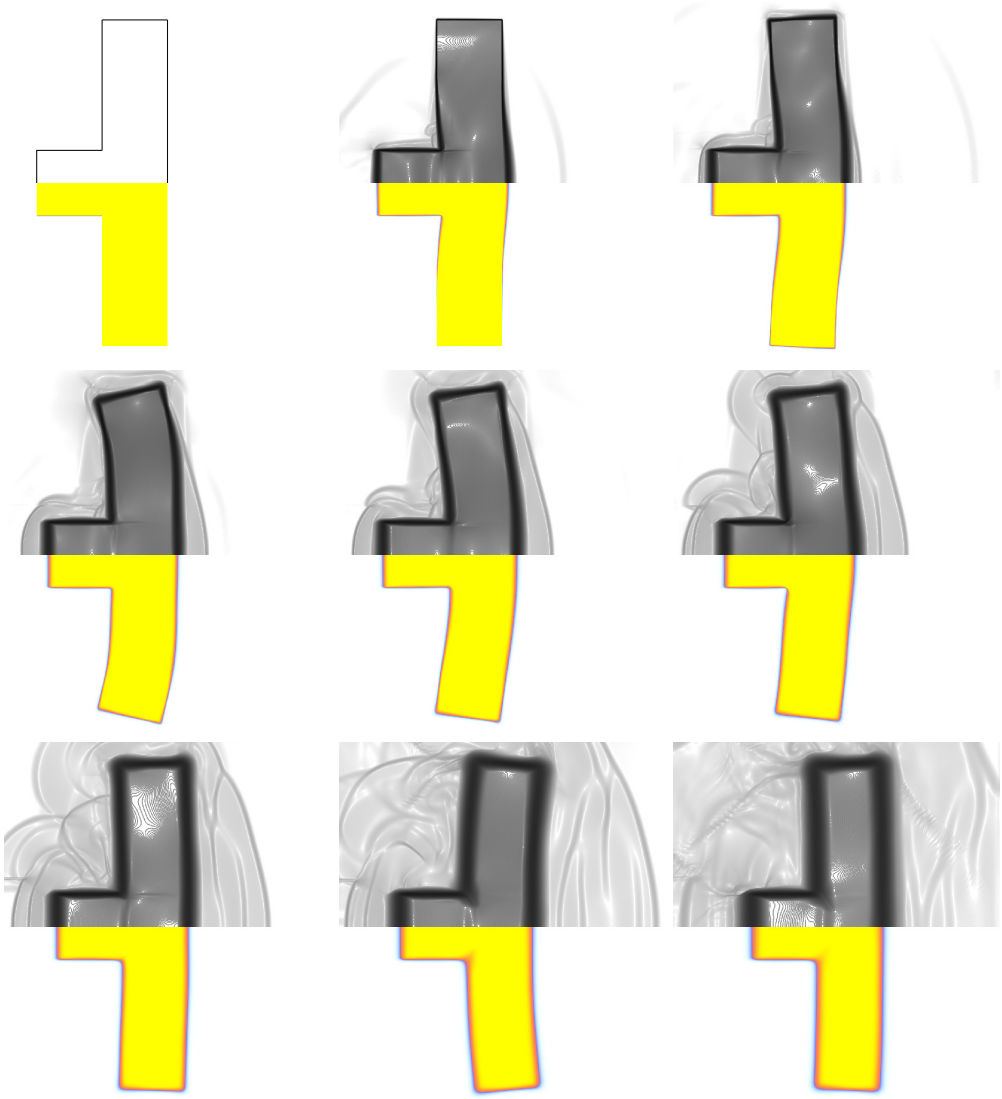

Figure 14: Impact of an elastic copper projectile on an elastic copper plate. The evolution of the projectile and the plate are shown through the volume fraction of copper and a schlieren of mixture density plotted at different instants: $t = 40\mu s$, $t = 70\mu s$, $t = 110\mu s$, $t = 200\mu s$, $t = 300\mu s$, $t = 490\mu s$ and $t = 700\mu s$.

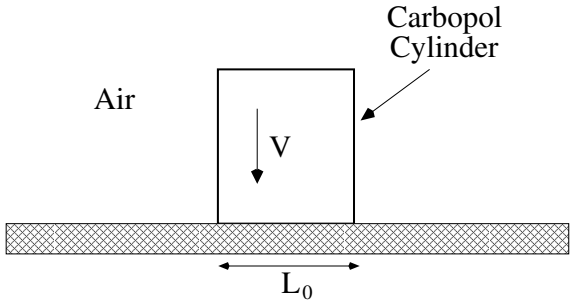

Figure 15: Impact of a carbopol droplet on a rigid wall : initial configuration.

can notice that the droplet computed with $a = -1$ continues to spread while the one computed with $a = 0$ begins to retract. Thus the final spreading of the droplets strongly depends on the parameter a.

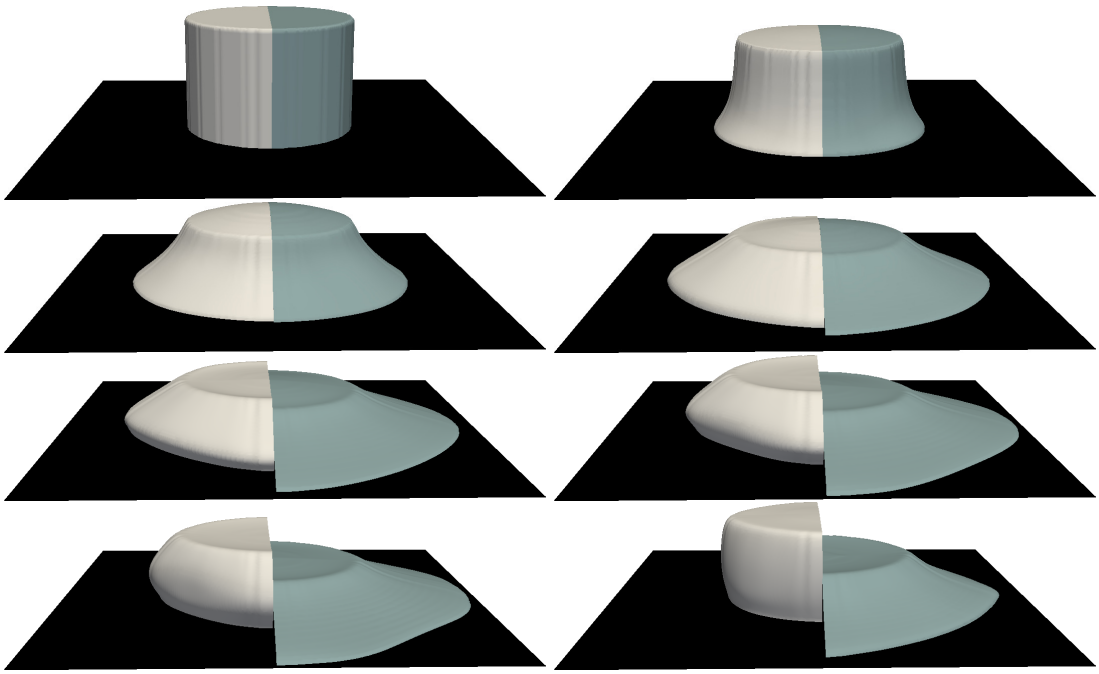

Figure 16: Numerical results for the impact of a carbopol droplet on a rigid wall. The results are represented at time $t = 0.5ms$, $t = 1.5ms$, $t = 3.0ms$, $t = 4.5ms$, $t = 6.0ms$, $t = 8.0ms$, and $t = 16.0ms$. Both computations are represented on the same Figure. The results using value $a = -1$ are plotted in blue (right side) and results associated to the value $a = 0$ are plotted in white (left side). The behaviours of droplets are different since $t > 1.5ms$

In order to compare our results with those obtained in [24]. Other computations have been performed with different impact velocities. Each of them has been made twice with two values of the parameter a. Results are summarized in the Figure 17. It is clear that the value of the parameter a of the elastic equation of state have a huge influence on the material behaviour. The value $a = -1$ corresponds to the case of neo-Hookean material (see the proof in[14]) The results are in good agreement.

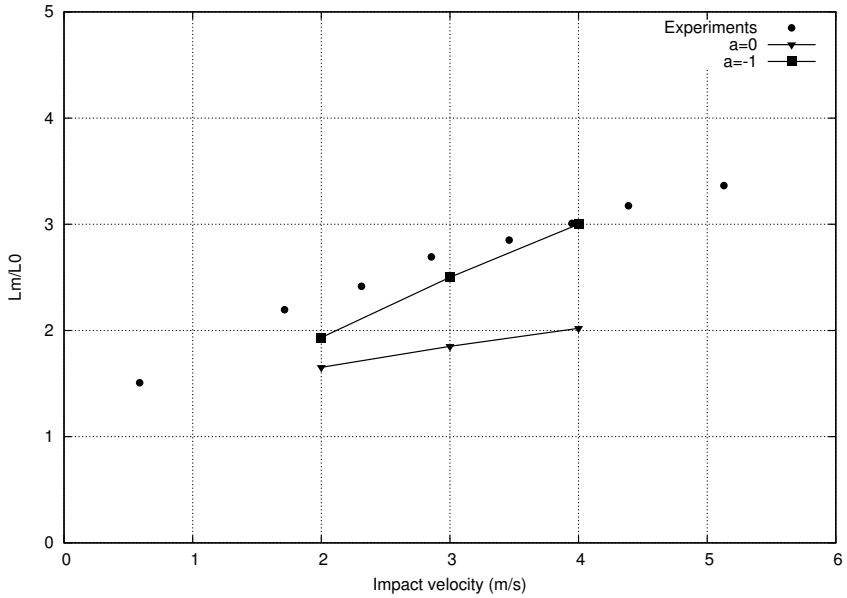

Figure 17: Impact of a carbopol droplet. Experimental results obtained by Luu and Fortere [24] are shown in circle and the numerical results are represented with squares and triangles.

6.3 Conservation of the vorticity constraint $curl(\mathbf{e}^{\beta}) = 0$

In this test case, we study the preservation of the constraint $curl(\mathbf{e}^{\beta}) = 0$. This test is performed in two dimensions of space. We consider here the test case proposed by [8] and described hereafter. The initial configuration is presented in Figure 18.

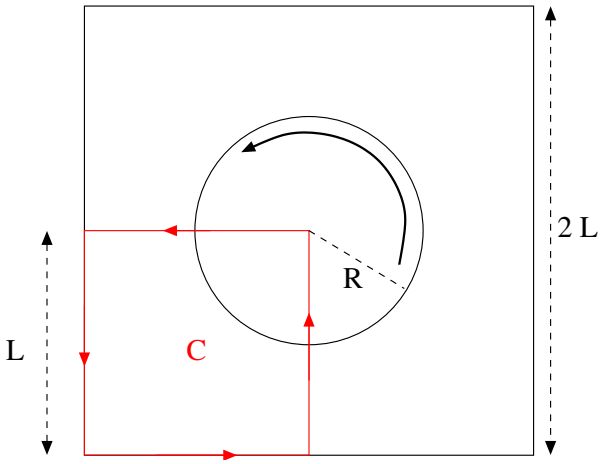

Figure 18: Initial configuration: A square containing pure solid is studied. Solid within the circle is in motion with a constant angular velocity while outside the circle, the solid is at rest. $L = 1m$ and $R = 0.5m$.

At initial time, a disc of elastic material is in rotation in the same elastic material at the angular

velocity $\omega = 4000 rad.s^{-1}$, the velocity field is :

$$\left(\begin{array}{c} u \\ v \end{array} \right)\Big|_{t=0} = \left\{ \begin{array}{l} \left(\begin{array}{c} -\omega y \\ \omega x \end{array} \right) , if\ x^2 + y^2 < R^2 \\ \left(\begin{array}{c} 0 \\ 0 \end{array} \right) , if\ x^2 + y^2 > R^2 \end{array} \right.$$

With such a choice, strong shear is present at the limit $x^2 + y^2 = R^2$, with a tangential jump of 2000 $m.s^{-1}$. The pressure and the density are represented in Figure 19 at time $t = 5\mu s$ and $t = 10\mu s$ on a 800×800 cells mesh. The circulation Γ, of the vector e^1 along the contour C is computed at time

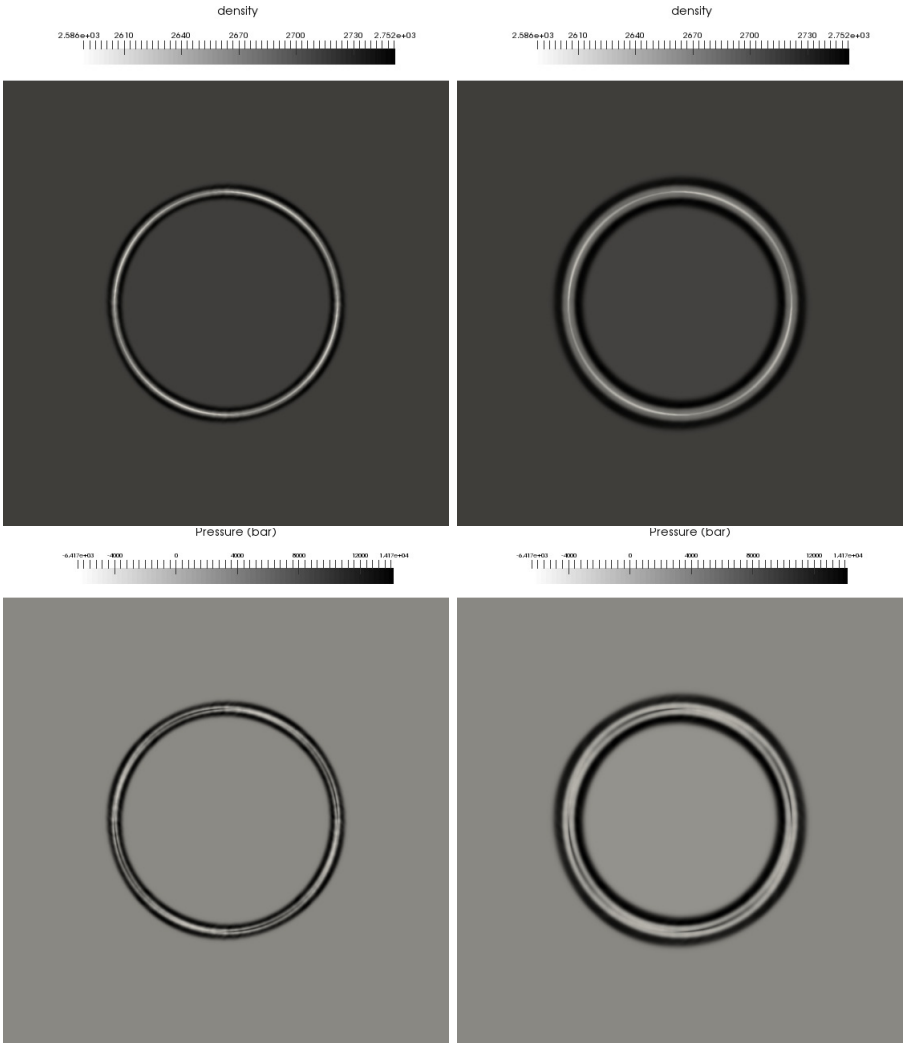

Figure 19: Density and pressure of the material at time $t = 5\mu s$ (on the left) and $t = 10\mu s$ (on the right).

$t = 10\mu s$. This contour C is a square of dimension $L = 1m$.

$$\Gamma = \oint_C a^1 dx + b^1 dy = \int\int_D \left(\frac{\partial b^1}{\partial x} - \frac{\partial a^1}{\partial y} \right) dxdy.$$

The follwowing dimensionless variables are introduced:

$$\tilde{\Gamma} = \frac{\Gamma}{L}, \quad \tilde{dx} = \frac{dx}{L}, \quad \tilde{dy} = \frac{dy}{L},$$

it comes

$$ln\left(\tilde{dx}\right) = ln\left(\tilde{dy}\right) = ln\left(\frac{2}{N}\right),$$

where N is the number of cells in each direction ($N_x = N_y = N$). In Figure 20, $ln(|\tilde{\Gamma}|)$ is represented as a function of $ln\left(\tilde{dx}\right)$ for different mesh sizes. The first order convergence is represented with a line. The developped numerical scheme preserved the vorticity constraint at first order.

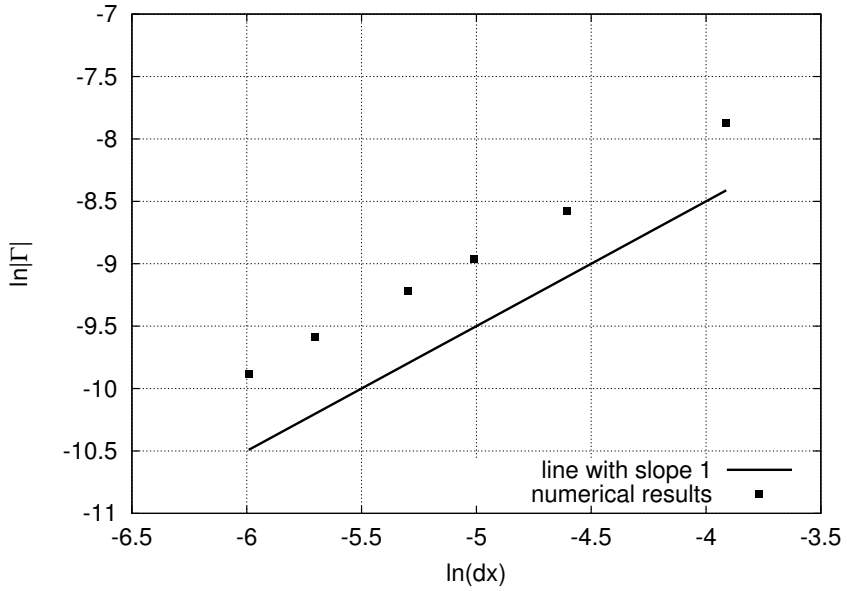

Figure 20: The circulation of the stationary constraint $curl(\mathbf{e}^1)$ at time $t = 10\mu s$: $ln(|\tilde{\Gamma}|)$ is represented as a function of the grid size. 100×100, 200×200, 300×300, 400×400, 600×600 and 800×800 cells mesh are considered. The first order convergence slope is represented with continuous line. The developed numerical scheme is able to preserve the vorticity constraint at first order.

7 Conclusions

An hyperbolic multiphase model with two pressures and two velocities for elastic solid-fluid coupling in Eulerian formulation has been developed. A splitting methods has been used to simplify the solving of the Riemann problem and decrease the numerical diffusion of the shear waves. The model is illustrated by two dimensional hypervelocity impact of solids and compared with a good agreament on experiment of droplet of jelly on a rigid surface. For high velocity impact on real metals and porous material, some more physics should be added for comparison on real experiments. Introduction of plasticity and compaction effects will be added on the basis of [11, 10] and [12] in a forthcoming paper.

Acknowledgments

The author thanks R.Abgrall and S. Gavrilyuk for fruitful discussion. This work was partially supported by ANR and A*MIDEX, France, the grants ANR-14-ASTR-0016-01, ANR-11-LABEX-0092 and ANR-11-IDEX-0001-02.

References

[1] R. Abgrall. How to prevent pressure oscillations in multicomponent flow calculations: a quasi conservative approach. Journal of Computational Physics, 125(1):150–160, 1996.

[2] R. Abgrall and R. Saurel. Discrete equations for physical and numerical compressible multiphase mixtures. Journal of Computational Physics, 186(2):361–396, 2003.

[3] M.R. Baer and J.W. Nunziato. A two-phase mixture theory for the deflagration-to-detonation transition (ddt) in reactive granular materials. International Journal of Multiphase Flows, 12(6):861–889, 1986.

[4] P.T. Barton, D. Drikakis, E. Romenski, and Titarev V.A. Exact and approximate solutions of riemann problems in non-linear elasticity. Journal of Computational Physics, 228(18):7046–7068, 2009.

[5] A. Chinnayya, E. Daniel, and R. Saurel. Modelling detonation waves in heterogeneous energetic materials. Journal of Computational Physics, 196(2):490–538, 2004.

[6] C. Czarnota, N. Jacques, S. Mercier, and A. Molinari. Modelling of dynamic ductile fracture and application to the simulation of plate impact tests on tantalum. Journal of the Mechanics and Physics of Solids, 56(4):1624–1650, 2008.

[7] S.F. Davis. Simplified second-order godunov-type methods. SIAM Journal on Scientific and Statistical Computing, 9(3):445–473, 1988.

[8] N. Favrie, S.L. Gavrilyuk, and S. Ndanou. A thermodynamically compatible splitting procedure in hyperelasticity. Journal of Computational Physics, 270:300–324, 2014.

[9] N. Favrie, S.L. Gavrilyuk, and R. Saurel. Solid-fluid diffuse interface model in cases of extreme deformations. Journal of Computational Physics, 228(16):6037–6077, 2009.

[10] N. Favrie and Gavrilyuk S.L. Dynamics of shock waves in elastic-plastic solids. ESAIM: Proceedings, 33(1947):50–67, 2011.

[11] N. Favrie and Gavrilyuk S.L. Mathematical and numerical model for nonlinear viscoplasticity. Philosophical Transactions of the Royal Society of London A: Mathematical, Physical and Engineering Sciences, 369(1947):2864–2880, 2011.

[12] N. Favrie and Gavrilyuk S.L. Dynamic compaction of granular materials. Proceedings of the Royal Society of London A: Mathematical, Physical and Engineering Sciences, 469(2160):20130214, 2013.

[13] P.J. Flory. Thermodynamic relations for high elastic materials. Trans. Faraday Soc., 57:829–838, 1961.

[14] S. Gavrilyuk, S. Ndanou, and Hank S. One-parameter family of equations of state for isotropic compressible solids. Accepted in Journal of Elasticity, 2015.

[15] S.L. Gavrilyuk, N. Favrie, and R. Saurel. Modelling wave dynamics of compressible elastic materials. Journal of Computational Physics, 227(5):2941–2969, 2008.

[16] S.K. Godunov and E.I. Romenskii. Elements of continuum mechanics and conservation laws. Springer Science & Business Media, 2003.

[17] J.O. Hallquist, G.L. Goudreau, and D. J. Benson. Sliding interfaces with contact-impact in large-scale lagrangian computations. Computer methods in applied mechanics and engineering, 51(1):107–137, 1985.

[18] AK. Kapila, SF. Son, JB. Bdzil, R. Menikoff, and DS Stewart. Two-phase modeling of ddt: Structure of the velocity-relaxation zone. Physics of Fluids (1994-present), 9(12):3885–3897, 1997.

[19] AK. Kapila, SF. Son, JB. Bdzil, R. Menikoff, and DS Stewart. Two-phase modeling of deflagration-to-detonation transition in granular materials: Reduced equations. Physics of Fluids (1994-present), 13(10):3002–3024, 2001.

[20] S. Karni. Multicomponent flow calculations by a consistent primitive algorithm. Journal of Computational Physics, 112(1):31–43, 1994.

[21] G. Kluth and B. Després. Perfect plasticity and hyperelastic models for isotropic materials. Continuum Mechanics and Thermodynamics, 20(3):173–192, 2008.

[22] A.G. Kulikovskii and E.I. Sveshnikova. Nonlinear waves in elastic media. CRC Press, 1995.

[23] O. Le Métayer, J. Massoni, and R. Saurel. Modelling evaporation fronts with reactive riemann solvers. Journal of Computational Physics, 205(2):567–610, 2005.

[24] L.H. Luu and Y. Forterre. Drop impact of yield-stress fluids. Journal of Fluid Mechanics, 632:301–327, 2009.

[25] G.H. Miller and P. Colella. A high-order eulerian godunov method for elastic–plastic flow in solids. Journal of Computational Physics, 167(1):131–176, 2001.

[26] S Ndanou, N Favrie, and S. Gavrilyuk. Criterion of hyperbolicity in hyperelasticity in the case of the stored energy in separable form. Journal of Elasticity, 115(1):1–25, 2014.

[27] S. Ndanou, N. Favrie, and S. Gavrilyuk. Multi-solid and multi-fluid diffuse interface model: Applications to dynamic fracture and fragmentation. Journal of Computational Physics, 295:523–555, 2015.

[28] S. Ndanou, N. Favrie, and Gavrilyuk S.L. The piston problem in hyperelasticity with the stored energy in separable form. Mathematics and Mechanics of Solids.

[29] Menikoff R. and Plohr B. J. The riemann problem for fluid flow of real materials. Rev. Modern Phys., 88:75–130, 1989.

[30] R. Saurel and R. Abgrall. A multiphase godunov method for compressible multifluid and multiphase flows. Journal of Computational Physics, 150(2):425–467, 1999.

[31] R. Saurel, S.L. Gavrilyuk, and F. Renaud. A multiphase model with internal degrees of freedom: application to shock–bubble interaction. Journal of Fluid Mechanics, 495:283–321, 2003.

[32] R. Saurel and O. Lemetayer. A multiphase model for compressible flows with interfaces, shocks, detonation waves and cavitation. Journal of Fluid Mechanics, 431:239–271, 2001.

[33] R. Saurel, F. Petitpas, and R. A. Berry. Simple and efficient relaxation methods for interfaces separating compressible fluids, cavitating flows and shocks in multiphase mixtures. Journal of Computational Physics, 228(5):1678–1712, 2009.

[34] VA Titarev, E Romenski, and EF Toro. Musta-type upwind fluxes for non-linear elasticity. International journal for numerical methods in engineering, 73(7):897–926, 2008.

[35] E. F. Toro. Riemann solvers and numerical methods for fluid dynamics: a practical introduction. Springer Science & Business Media, 2009.

A Hyperbolicity of sub model 1

Sub-model 1 can be rewritten in a quasi-linear formulation,

$$\mathbf{W}_t + A(\mathbf{W})\mathbf{W}_x = 0.$$

Source terms are omitted. $\mathbf{W}$ is the vector of primitives variables:

$$\mathbf{W} = (\alpha_k, \rho_k, u_k, v_k, w_k, a_k^1, a_k^2, a_k^3, b_k^1, b_k^2, b_k^3, c_k^1, c_k^2, c_k^3, \eta)^T,$$

$A(\mathbf{W})$ is the jacobian matrix of the system. The eigenvalues of this matrix are the characteristic velocities of the system.

$$A(\mathbf{W}) = \begin{pmatrix} A_{11} & A_{12} \\ A_{21} & A_{22} \end{pmatrix}$$

With,

$$A_{11} = \begin{pmatrix} u_I & 0 & 0 \\ \dfrac{\rho_k}{\alpha_k}(u_k - u_I) & u_k & \rho_k \\ \dfrac{\sigma_{11_k} - \sigma_{11_I}}{\alpha_k \rho_k} & \dfrac{\left(\dfrac{\partial P_k}{\partial \rho_k} - \dfrac{\partial S_{11_k}}{\partial \rho_k}\right)}{\rho_k} & u_k \end{pmatrix}$$

$$A_{12} = \frac{1}{\rho_k}\begin{pmatrix} 0 & 0 & 0 & 0 & 0 & 0 & 0 & 0 & 0 & 0 & 0 & 0 \\ 0 & 0 & 0 & 0 & 0 & 0 & 0 & 0 & 0 & 0 & 0 & 0 \\ 0 & 0 & -\dfrac{\partial S_{11_k}}{\partial a^1} & -\dfrac{\partial S_{11_k}}{\partial a^2} & -\dfrac{\partial S_{11_k}}{\partial a^3} & -\dfrac{\partial S_{11_k}}{\partial b^1} & -\dfrac{\partial S_{11_k}}{\partial b^2} & -\dfrac{\partial S_{11_k}}{\partial b^3} & -\dfrac{\partial S_{11_k}}{\partial c^1} & -\dfrac{\partial S_{11_k}}{\partial c^2} & -\dfrac{\partial S_{11_k}}{\partial c^3} & \dfrac{\partial P}{\partial \eta} \end{pmatrix}$$

$$A_{21} = \begin{pmatrix} 0 & 0 & 0 \\ 0 & 0 & 0 \\ \dfrac{a_k^1}{\alpha_k}(u_k - u_I) & 0 & a_k^1 \\ \dfrac{a_k^2}{\alpha_k}(u_k - u_I) & 0 & a_k^2 \\ \dfrac{a_k^3}{\alpha_k}(u_k - u_I) & 0 & a_k^3 \\ 0 & 0 & 0 \\ 0 & 0 & 0 \\ 0 & 0 & 0 \\ 0 & 0 & 0 \\ 0 & 0 & 0 \\ 0 & 0 & 0 \\ 0 & 0 & 0 \\ 0 & 0 & 0 \end{pmatrix}, \qquad A_{22} = u_k \mathbb{I}_{12\times 12}$$

The Jacobian matrix admits 15 real eigenvalues:

$$\lambda_1 = u_k,\ \lambda_1 \text{ is of multiplicity 12},$$
$$\lambda_2 = u_I\ ,$$

$$\lambda_3 = u_k + \sqrt{\frac{\partial P_k}{\partial \rho_k} - \frac{\partial S_{11_k}}{\partial \rho_k} - \frac{1}{\rho_k}\frac{\partial S_{11_k}}{\partial \mathbf{a}}.\mathbf{a}}$$
$$\lambda_4 = u_k - \sqrt{\frac{\partial P_k}{\partial \rho_k} - \frac{\partial S_{11_k}}{\partial \rho_k} - \frac{1}{\rho_k}\frac{\partial S_{11_k}}{\partial \mathbf{a}}.\mathbf{a}}$$

The matrix admits 15 right eigenvectors linearly independant, and 15 eigenvalues, the system is hyperbolic. λ_3 and λ_4 are the characteristic of the two longitudinal waves.

B Hyperbolicity of sub model 2 and 3

Sub-system 2 can be rewritten in the quasi-linear form:

$$\mathbf{W}_t + B(\mathbf{W})\mathbf{W}_x = 0.$$

Source terms are omitted. $\mathbf{W}$ is the vector of primitives variables:

$$\mathbf{W} = (\alpha_k, \rho_k, u_k, v_k, w_k, a_k^1, a_k^2, a_k^3, b_k^1, b_k^2, b_k^3, c_k^1, c_k^2, c_k^3, \eta)^T.$$

$$B(\mathbf{W}) = \begin{pmatrix} B_{11} & B_{12} \\ B_{21} & B_{22} \end{pmatrix}$$

With,

$$B_{11} = \begin{pmatrix} 0 & 0 & 0 & 0 \\ 0 & 0 & 0 & 0 \\ 0 & 0 & 0 & 0 \\ \dfrac{\sigma_{12_k}}{\alpha_k \rho_k} & -\dfrac{1}{\rho_k}\dfrac{\partial S_{12_k}}{\partial \rho_k} & 0 & 0 \end{pmatrix}$$

$$B_{12} = \frac{1}{\rho_k}\begin{pmatrix} 0 & 0 & 0 & 0 & 0 & 0 & 0 & 0 & 0 & 0 & 0 \\ 0 & 0 & 0 & 0 & 0 & 0 & 0 & 0 & 0 & 0 & 0 \\ 0 & 0 & 0 & 0 & 0 & 0 & 0 & 0 & 0 & 0 & 0 \\ 0 & -\dfrac{\partial S_{12_k}}{\partial a^1} & -\dfrac{\partial S_{12_k}}{\partial a^2} & -\dfrac{\partial S_{12_k}}{\partial a^3} & -\dfrac{\partial S_{12_k}}{\partial b^1} & -\dfrac{\partial S_{12_k}}{\partial b^2} & -\dfrac{\partial S_{12_k}}{\partial b^3} & -\dfrac{\partial S_{12_k}}{\partial c^1} & -\dfrac{\partial S_{12_k}}{\partial c^2} & -\dfrac{\partial S_{12_k}}{\partial c^3} & 0 \end{pmatrix}$$

$$A_{21} = \begin{pmatrix} 0 & 0 & 0 & 0 \\ 0 & 0 & 0 & b_k^1 \\ 0 & 0 & 0 & b_k^2 \\ 0 & 0 & 0 & b_k^3 \\ 0 & 0 & 0 & 0 \\ 0 & 0 & 0 & 0 \\ 0 & 0 & 0 & 0 \\ 0 & 0 & 0 & 0 \\ 0 & 0 & 0 & 0 \\ 0 & 0 & 0 & 0 \\ 0 & 0 & 0 & 0 \end{pmatrix}, \qquad B_{22} = \mathbb{O}_{11\times 11}$$

With $\mathbb{O}_{11\times 11}$, the zero square matrix. The eigenvalues of the matrix B are the following:

$$\lambda_1 = \sqrt{-\frac{1}{\rho_k}\frac{\partial S_{12_k}}{\partial \mathbf{a}}.\mathbf{b}} \qquad , \lambda_2 = -\sqrt{-\frac{1}{\rho_k}\frac{\partial S_{12_k}}{\partial \mathbf{a}}.\mathbf{b}} \qquad , \lambda_3 = 0.$$

λ_3 is of multiplicity 13, the system admits 15 eigenvalues and 15 eigenvectors. It can be concluded that the sub system 2 is hyperbolic. The same computation can be made with sub system 3, and the conclusions are similar: Sub system 3 is hyperbolic and its characteristic velocities are:

$$\lambda_1 = \sqrt{-\frac{1}{\rho_k}\frac{\partial S_{13_k}}{\partial \mathbf{a}}.\mathbf{c}} \qquad , \lambda_2 = -\sqrt{-\frac{1}{\rho_k}\frac{\partial S_{13_k}}{\partial \mathbf{a}}.\mathbf{c}} \qquad , \lambda_3 = 0.$$

C Jump relations for sub-systems 2 and 3 Riemann problems

Jump relations associated to sub-system 2 are presented hereafter

$$\begin{cases} \sigma_{12}^* = \dfrac{S_r\rho_r\sigma_{12_l} - S_l\rho_l\sigma_{12_r} + S_r\rho_r S_l\rho_l(v_l - v_r)}{S_r\rho_r - S_l\rho_l} \\ v_r^* = v_r + \dfrac{\sigma_{12_r} - \sigma_{12^*}}{S_r\rho_r} \\ v_l^* = v_l + \dfrac{\sigma_{12_l} - \sigma_{12^*}}{S_l\rho_l} \\ \mathbf{a}_r^{\beta *} = \mathbf{a}_r^\beta + \mathbf{b}_r^\beta \dfrac{v_r^* - v_r}{S_r} \\ \mathbf{a}_l^{\beta *} = \mathbf{a}_l^\beta + \mathbf{b}_l^\beta \dfrac{v_l^* - v_l}{S_l} \\ E_r^* = E_r + \dfrac{\sigma_{12_r} v_r - \sigma_{12^*} v_r^*}{S_r\rho_r} \\ E_l^* = E_l + \dfrac{\sigma_{12_l} v_l - \sigma_{12^*} v_l^*}{S_l\rho_l} \end{cases}$$

Jump relations associated to the sub system 3 are quite similar,

$$\begin{cases} \sigma_{13}^* = \dfrac{S_r\rho_r\sigma_{13_l} - S_l\rho_l\sigma_{13_r} + S_r\rho_r S_l\rho_l(w_l - w_r)}{S_r\rho_r - S_l\rho_l} \\ w_r^* = w_r + \dfrac{\sigma_{13_r} - \sigma_{13^*}}{S_r\rho_r} \\ w_l^* = w_l + \dfrac{\sigma_{13_l} - \sigma_{13^*}}{S_l\rho_l} \\ \mathbf{a}_r^{\beta *} = \mathbf{a}_r^\beta + \mathbf{c}_r^\beta \dfrac{w_r^* - w_r}{S_r} \\ \mathbf{a}_l^{\beta *} = \mathbf{a}_l^\beta + \mathbf{c}_l^\beta \dfrac{w_l^* - w_l}{S_l} \\ E_r^* = E_r + \dfrac{\sigma_{12_r} w_r - \sigma_{13^*} w_r^*}{S_r\rho_r} \\ E_l^* = E_l + \dfrac{\sigma_{13_l} w_l - \sigma_{13^*} w_l^*}{S_l\rho_l} \end{cases}$$